High-pressure study of a natural cancrinite

Revision_1

High-pressure study of a natural cancrinite

Corresponding author: G. Diego GATTA

Dipartimento di Scienze della Terra

Universita' degli Studi di Milano

Via Botticelli, 23

I-20133 Milano, Italy

E-Mail: diego.gatta@unimi.it

High-pressure study of a natural cancrinite

Paolo Lotti[1], G. Diego Gatta [1,2], Nicola Rotiroti[1,2], Fernando Cámara[3]

[1]*Dipartimento di Scienze della Terra - Università degli Studi di Milano, Via Botticelli 23, 20133 Milano, Italy*

[2] *CNR - Istituto per la Dinamica dei Processi Ambientali, Via M. Bianco 9, 20131 Milano, Italy*

[3]*Dipartimento di Scienze Mineralogiche e Petrologiche - Università degli Studi di Torino, Via Valperga Caluso 35, 10125 Torino, Italy*

Abstract

The high-pressure behavior and the *P*-induced structure evolution of a natural cancrinite from Cameroun ($Na_{6.59}Ca_{0.93}[Si_6Al_6O_{24}](CO_3)_{1.04}F_{0.41}\cdot 2H_2O$, a = 12.5976(6) Å, c =5 .1168(2) Å, space group: $P6_3$) were investigated by *in situ* single-crystal X-ray diffraction under hydrostatic conditions up to 6.63(2) GPa with a diamond anvil cell. The *P*-*V* data were fitted with an isothermal Birch-Murnaghan-type equation of state (BM EoS) truncated to the 3rd-order. Weighted fit (by the uncertainty in *P* and *V*) gave the following elastic parameters: V_0 = 702.0(7) Å^3, K_{V0} = 51(2) GPa and K_V' = 2.9(4). Linearized BM EoS was used to fit the *a*-*P* and *c*-*P* data, giving the following refined parameters: a_0 = 12.593(5) Å, K_{a0} = 64(4) GPa, K_a' = 4.5(9), for the *a*-axis, and c_0 = 5.112(3) Å, K_{c0} = 36(1) GPa, K_c' = 1.9(3) for the *c*-axis (elastic anisotropy: K_{a0}:K_{c0} = 1.78:1). A subtle change of the elastic behavior appears to occur at P > 4.62 GPa, and so the elastic behavior was also described on the basis of BM EoS valid between 0.0001 – 4.62 and 5.00 – 6.63 GPa, respectively. The high-pressure structure refinements allowed the description of the main deformation mechanisms responsible for the anisotropic compression of cancrinite on (0001) and along [0001]. A comparative analysis of the structure evolution in response of the applied pressure and temperature of isotypic materials with cancrinite-like topology is carried out.

Keywords: cancrinite, zeolites, high pressure, compressibility, structure evolution.

Introduction

Cancrinite is a feldspathoid with ideal chemical formula $(Na,Ca)_{7\text{-}8}[Al_6Si_6O_{12}](CO_3)_{1.2\text{-}1.7}\cdot 2H_2O$, which can form as a primary phase in low-SiO_2 alkaline rocks in the late hydrothermal stages or as the

alteration product of nepheline- or sodalite-group minerals. It is the parent member of a group including about 20 minerals (Bonaccorsi and Merlino 2005; Cámara et al. 2005; Rastvetaeva et al. 2007; Cámara et al. 2010; Bonaccorsi et al. 2012), among which the most common are davyne and vishnevite.

Cancrinite has an open-framework structure (framework density = 16.9 T/1000 $Å^3$, Baerlocher et al. 2007), with CAN topology. Its framework is built up by 12-, 6- and 4-membered rings of tetrahedra in a way that planes of 6-membered rings perpendicular to [0001] (hereafter 6mRs⊥[0001]) are stacked according to an ··ABAB·· close-packing sequence (Fig. 1). The resulting framework consists of columns of base-sharing cages (Fig. 1), the so-called cancrinite, or undecahedral or ε cages (Baerlocher et al. 2007), and iso-oriented 12mRs-channels parallel to [0001] (Figs. 1, 2). Cages and channels are connected by distorted 6mRs windows parallel to [0001] (hereafter 6mR//[0001]) (Fig. 2). Moreover, 4mRs form *double zigzag chains* (Baerlocher et al. 2007) running parallel to [0001] (Fig. 1). The topological symmetry of the CAN framework type is $P6_3/mmc$, with idealized lattice constants a = 12.494 Å and c = 5.254 Å (Baerlocher et al. 2007).

The cancrinite structure was first described by Pauling (1930) and then refined by Jarchow (1965) in the space group $P6_3$, due to the full Si/Al-ordering in the tetrahedral framework. The extra-framework population consists of ···Na–H_2O—Na–H_2O··· chains lying in the cancrinite cages and by CO_3^{2-} groups lying in two mutually exclusive and partially occupied positions in the center of the 12mRs-channels, occupied also by mixed Na/Ca sites near the channel wall (Figs. 3 and 4). In cancrinite the ···Na–H_2O–Na··· chains show one shorter and one longer Na-H_2O bond distances. In contrast, in the isotypic davyne or microsommite (Bonaccorsi and Merlino 2005), ···Ca-Cl··· chains show constant bond lengths. In the 12mRs-channel, different anions (*e.g.* SO_4^{2-}, NO_3^-, Cl^-, OH^-) or H_2O molecules can replace CO_3^{2-} in natural or synthetic cancrinites (*e.g.* Grundy and Hassan 1982; Hassan and Grundy 1984; Bresciani-Pahor et al. 1982; Hassan and Grundy 1991; Buhl et al. 2000; Fechtelkord et al. 2001; Ballirano and Maras 2005).

Over the last forty years, cancrinite-like materials have been extensively studied for their structure-related properties. Many studies have been devoted to the superstructures reflections often found in cancrinites, governed by the ordering of the carbonate groups and their vacancies along [0001] (*e.g.* Grundy and Hassan 1982; Brown and Cesbron 1973; Foit et al. 1973; Hassan and Buseck 1992), but also for the occurrence and use of cancrinite in many technological processes: *e.g.* as final product

of Na-aluminosilicates precipitation from liquor during the Bayer process for the refining of bauxite (Gerson and Zheng 1997; Barnes et al. 1999) or as a precipitation product in nuclear waste tanks at the Hanford site (WA, USA), and as product of the reaction between simulated leaked waste fluids and quartz- or kaolinite-bearing sediments at the same site (Buck and McNamara 2004; Bickmore et al. 2001; Zhao et al. 2004). Moreover, Zhao et al. (2004) reported a sorption capacity for Cs^+ ions in waste fluids, whereas Poborchii (1994) and Poborchii et al. (2002) studied the optical properties of Se_2^{2-} and Se_2^- in the cancrinite channels.

Only a few studies have been devoted to the behavior of cancrinite under non-ambient conditions. Hassan et al. (2006) performed an *in-situ* high-temperature X-ray powder diffraction study up to 1255 K, and reported: 1) a phase transition with loss of the superstructure reflections at ~777 K, 2) a continuous dehydration process toward a full dehydration at 898 K coupled with 3) a minimal loss of CO_2. The results of an *in-situ* high-temperature single-crystal X-ray diffraction study up to 673 K were reported by Isupova et al. (2010), whereas the description of the elastic behavior and structure evolution at low-temperature (L*T*) conditions (down to 100 K) was recently provided by Gatta et al. (2011) by *in-situ* L*T* single-crystal X-ray diffraction. Gatta and Lee (2008) described the elastic behavior and the pressure-induced structure evolution of $Na_6Cs_2Ga_6Ge_6O_{24}{\cdot}Ge(OH)_6$, a synthetic compound isotypic with cancrinite, by means of *in-situ* high pressure (H*P*) synchrotron powder diffraction up to 5.01 GPa. However, to the best of our knowledge, no study has to date been devoted to the H*P* behavior of a natural cancrinite. In this light, the aim of this study is to describe the elastic behavior and the *P*-induced structure evolution of a natural cancrinite, with no evidence of superstructure reflections at ambient conditions, by *in-situ* single-crystal X-ray diffraction under hydrostatic conditions. The formulation of the isothermal equation of state, along with the description of the main deformation mechanisms of the tetrahedral framework and the behavior of the extra-framework population will be provided. Furthermore, a comparative analysis of the structure evolution in response of the applied pressure of the natural cancrinite here investigated and of $Na_6Cs_2Ga_6Ge_6O_{24}{\cdot}Ge(OH)_6$ (Gatta and Lee 2008) will be carried out.

Materials and methods

The single-crystal X-ray diffraction experiments were performed on a platy crystal of natural cancrinite free of defects under the polarized microscope, collected from the same gem-quality sample from

Cameroun used by Della Ventura et al. (2009), for a single-crystal neutron diffraction experiment and polarized infra-red spectroscopy, and by Gatta et al. (2011), for a L*T* single-crystal X-ray diffraction study. Cancrinite crystals from this sample do not show any evidence of superstructure reflections. The chemical composition, obtained by electron microprobe analysis in wavelength dispersive mode, is $Na_{6.59}Ca_{0.93}[Si_6Al_6O_{24}](CO_3)_{1.04}F_{0.41}\cdot 2H_2O$ (Z = 1) (Della Ventura et al. 2009).

An intensity data collection with the crystal in air was first performed using an Xcalibur - Oxford Diffraction diffractometer equipped with a CCD detector, operating at 50 kV and 40 mA with a monochromatised Mo*K*α radiation source and a detector-sample distance fixed at 80 mm. A combination of ω and φ scans was chosen to maximize data coverage and redundancy. The step scan was 1°/frame along with an exposure time of 60 s/frame (Table 1). A total number of 19,933 reflections, out of which 1933 unique for symmetry, were collected up to $2\theta_{max}$=70°, showing a metrically hexagonal lattice with systematic extinctions consistent with the space group $P6_3$ (Table 1). The refined unit-cell parameters were: a = 12.5976(6) Å, c = 5.1168(2) Å and V = 703.2(1) Å^3 (Table 1). Intensities were then integrated, corrected for Lorentz-polarization (Lp) and for absorption effects (analytical absorption corrections by Gaussian integration based upon the physical description of the crystal) using the CrysAlis software package (Oxford Diffraction 2010). Further details pertaining to the data collection strategy are in Table 1. A hydrogen-free structure refinement of cancrinite was then performed with the Shelx-97 program (Sheldrick 1997), starting from the atomic coordinates of Della Ventura et al. (2009) in the space group $P6_3$. Neutral atomic scattering factors for Si, Al, Na, Ca, C and O from the *International Tables of Crystallography* (Wilson and Prince 1999) were used. A mixed scattering curve of Na and Ca was used to model the *Na*2 site, and the site occupancy factors of *C*1 and *C*2 were constrained to be equal to that of *Oc*1 and *Oc*2, respectively. The H_2O oxygen site (*Ow*), lying off the 3-fold axis in three symmetry-related and mutually exclusive positions, was modeled with a site occupancy factor (s.o.f.) of 1/3. The *C-Oc* bond lengths were restrained to 1.300 ± 0.005 Å, on the basis of the neutron refinement reported by Della Ventura et al. (2009). In the last cycles of the refinement, the displacement parameters of all the atomic sites were refined anisotropically; only *C*, *Oc* and *Ow* sites were refined isotropically, due to a significant correlation among the refined parameters likely ascribable to the positional disorder of the carbonate groups and H_2O molecules (Grundy and Hassan 1982; Della Ventura et al. 2009). The refinement converged to an agreement factor R_1 of 5.6% for 1092 reflections with $F_o > 4\sigma(F_o)$. At the end of the refinement, no significant correlation was observed in the variance-covariance matrix and the residual peaks in the difference-Fourier function of

the electron density were between +0.77/-0.55 e^-/Å^3. Further details pertaining to the structure refinement are in Table 1.

An ETH-type diamond anvil cell (DAC, Miletich et al. 2000), was used for the high-pressure experiments. A T301 steel foil, 0.250 mm thick, was used as a gasket, which was pre-indented to a thickness of about 0.110 mm before drilling a micro-hole (~ 0.300 mm in diameter) by spark-erosion. The same crystal of cancrinite previously investigated at ambient conditions was placed into the gasket hole along with some ruby chips and a single-crystal of quartz used as *P*-standards (Mao et al. 1986; Angel et al. 1997). A 4:1 mixture of methanol:ethanol was used as hydrostatic pressure-transmitting medium (Angel et al. 2007). Lattice parameters were measured between 0.0001 and 6.63(2) GPa (Table 2), using 42 Bragg reflections with a KUMA KM4 point-detector diffractometer, operating at 50 kV and 40 mA with a graphite monochromatized Mo*K*α radiation source. Ten intensity data collections between 0.0001 GPa (with crystal in the DAC without any pressure medium) and 6.63(3) GPa (Table 1) were performed with an Xcalibur - Oxford Diffraction diffractometer equipped with a CCD (graphite-monochromatized Mo*K*α radiation). A combination of ω and φ scans was used, with step of 0.5 °/frame and an exposure time of 60 s/frame (Table 1). No violations of the reflection conditions expected for the space group $P6_3$ were observed within the *P*-range investigated. Integrated intensity data were corrected for Lp and absorption effects due to the crystal and the DAC using the ABSORB computer program (Angel 2004). The H*P* structure refinements based on the intensity data collected with the crystal in the DAC were performed with the Shelx-97 program (Sheldrick 1997). The number of the refined parameters was reduced to 45: all the occupancy factors were constrained to the values refined with the crystal in air and the atomic displacement parameters (a.d.p.s.) were all refined isotropically. In addition, the *C*1-*C*2 and *Oc*1-*Oc*2 a.d.p.s. were, respectively, constrained to be equal. As for the structure model at room conditions, the *C*-*Oc* bond lengths were restrained to 1.300 ± 0.005 Å^3. The refinements converged for all the H*P* datasets with R_1 always lower than 8.9%, with no significant correlation between the refined parameters and residual peaks in the difference-Fourier maps lower than ±0.96 e^-/Å^3.

Atomic fractional coordinates, site occupancy factors and atomic displacement parameters pertaining to the structure refinements at room-*P* and H*P* are given in Table 3; bond distances and angles are listed in Table 4. Refined anisotropic displacement parameters are available in the CIF (deposited).

Results

Elastic behavior

The evolution of the unit-cell parameters of cancrinite up to 6.63(2) GPa is shown in Fig. 5. The unit-cell parameters measured in decompression showed that the pressure-induced structural evolution of up to ~6.6 GPa is completely reversible.

The *P*-*V* between 0.0001 and 6.63 GPa data were first fitted with an isothermal Birch-Murnaghan-type equation of state truncated to the 3rd-order (BM-III EoS, Birch 1947), using the EoS-Fit v5.2 program (Angel 2000). Weighted fit (by the uncertainty in *P* and *V*) gives the following elastic parameters: V_0 = 702.0(7) Å^3, K_{V0} = 51(2) GPa and K_V' = 2.9(4). The evolution of the Eulerian strain *vs.* the normalized pressure within the entire *P*-range investigated (*fe*-*Fe* plot, $f_e = [(V_0/V)^{2/3} - 1]/2$ and $F_e = P/[3f_e(1+2f_e)^{5/2}]$, Angel 2000) is shown in Fig. 5, suggesting that the isothermal volume compression in cancrinite can be described with a 3rd-order BM EoS, giving a bulk modulus at room-*P* of *Fe*(0) = 50(1) and its *P*-derivative of 3.2(3). A "linearized" BM-III equation of state was used to fit the *a*-*P* and *c*-*P* data (Angel 2000), giving the following refined parameters: a_0 = 12.593(5) Å, K_{a0} = 64(4) GPa, K_a' = 4.5(9), c_0 = 5.112(3) Å, K_{c0} = 36(1) GPa, K_c' = 1.9(3). The elastic anisotropy at room pressure is then: K_{a0}:K_{c0} = 1.78:1.

When one EoS is used over the entire *P*-range investigated, a modest misfit is observed for the *a*-axis and the unit-cell volume, respectively, suggesting a potential change of the compressional behaviors between 4.62 – 5.00 GPa. On this basis, two different BM EoS fits were used to model the elastic behavior along the *a*-axis and for the unit-cell volume between 0.0001 – 4.62 and 5.00 – 6.63 GPa, respectively. The refined parameters are: a_0 = 12.603(7) Å, K_{a0} = 52(6) GPa and K_a' = 11(4), and V_0 = 703.3(7) Å^3, K_{V0} = 45(2) GPa and K_V' = 6(1) between 0.0001 and 4.62 GPa; a_0 = 12.63(2) Å, K_{a0} = 58(4) GPa and K_a' = 4 (fixed), and V_0 = 715(4) Å^3, K_{V0} = 40(2) GPa and K_V' = 4 (fixed) between 5.00 and 6.63 GPa. A further *fe*-*Fe* plot is shown in Fig. 5 with the refined V_0 obtained by the BM-III EoS fit (0.0001 – 4.62 GPa) and by the BM-II EoS fit (5.00 – 6.63 GPa), respectively.

Structure refinements

The structure refinement of cancrinite at room-*P* confirms the framework and extraframework configuration previously described (*e.g.* Della Ventura et al. 2009), with the ε cages stuffed by ···Na–H_2O—Na–H_2O··· chains and the 12mRs-channels with cation sites close to the channel walls (*Na*2), partially occupied by Na (85.4(6)%) and Ca (14.6(6)%), and CO_3^{2-} groups in the center of the channel in two mutually exclusive positions (*i.e. C*1 and *Oc*1 s.o.f. = 42.1(7)%; *C*2 and *Oc*2 s.o.f = 45.9(6)%; Table 3) (Figs. 3, 4). The chemical formula deduced on the basis of the structure refinement is: $Na_{7.04}Ca_{0.88}[Al_6Si_6O_{24}](CO_3)_{1.76}\cdot 2H_2O$, and if we consider the amount of F obtained on the basis of the EMPA-EDS (*i.e.* 0.41 atoms per formula unit, Della Ventura et al. 2009), we obtain (after a recalculation of the C/F s.o.f.): $Na_{7.04}Ca_{0.88}[Al_6Si_6O_{24}](CO_3)_{1.15}F_{0.41}\cdot 2H_2O$. This chemical formula shows a slightly higher amount of Na and a lower amount of Ca with respect to the formula reported by Della Ventura et al. (2009). In fact, the sum of the electrons ascribable to the extraframework cations (Na and Ca) from the structure refinement is 95.4 e^-, slightly higher than 91.1 e^- from the experimental chemical analysis (Δe^- ~ 4.5%).

The H*P* structure refinements showed that the general configuration of framework and extraframework population was maintained within the *P*-range investigated; the main deformation mechanisms of the tetrahedral framework and of the channel and cage content are described below.

High-pressure framework behavior

At high pressure, the structure refinements show that the 6-membered rings perpendicular to [0001] (6mRs⊥[0001]) experience a ditrigonalization process, with the opening of the ω1 angle (*O*1-*O*2-*O*1) and the closure of ω2 angle (*O*2-*O*1-*O*2) (Fig. 2; Table 4). A linear increasing of the ditrigonal rotation angle α (Fig. 6; Table 4) [$\alpha = 1/6\cdot\Sigma_i|120° - \theta_i|/2$, where θ_i is the angle between the basal edges of neighboring tetrahedra articulated in the six membered ring; Brigatti and Guggenheim 2002] is observed. This unit is also compressed in response to the applied pressure as shown by the shortening of the *O*1-*O*2 distance and the reduction of the ditrigonal area subtended by the oxygen atoms (Fig. 2; Table 4). Moreover, we observed a decrease of the (A,B)-plane corrugation [defined as $\Delta z = [z(O)_{max} - z(O)_{min}]\cdot c$, where $z(O)_{max}$ is the maximum *z* coordinate of the oxygen atoms belonging to the plane, $z(O)_{min}$ the minimum one and *c* is the unit-cell edge length; Brigatti and Guggenheim 2002)] (Table 4).

The 4mR joint-unit shows a compression along the *O*3-*O*4 diameter (Figs. 2 and 6; Table 4), whereas an expansion is shown along *O*2-*O*2, giving as overall effect a reduction of the area subtended by the four oxygen corners (Fig. 2; Table 4). In the 12mR-channel, an almost constant value of the six symmetrically related *O*3-*O*4 distances is observed with pressure, along with a shortening of the six symmetrical *O*1-*O*1 distances (*i.e.* ~5.7%; Figs. 2 and 6; Table 4). The 6mR-windows connecting channels and cages (6mR//[0001]) show a strong ditrigonalization with a shortening of the *O*1-*O*1 diameter (*i.e.* the *c* edge of unit-cell), and a less pronounced contraction of the *O*3-*O*3 and *O*4-*O*4 diameters (Fig. 2; Table 4). The cancrinite cage shows a pronounced flattening along [0001], governed by the closure of the κ angle (*O*2-*O*2-*O*2) (Figs. 2 and 6; Table 4), whereas the maximum width on the (0001) plane, defined by the three symmetry-related diameters *O*2-*O*2 (dashed lines in Fig. 2), is constant within the *P*-range investigated (Table 4).

The evolution of the channel volume (modeled as $V_{ch} = D \cdot c$; with D = (*O*1-*O*1 + *O*3-*O*4)/2, where *O*1-*O*1 and *O*3-*O*4 are the independent diameters of the 12mR; Fig. 2, Table 4) and of the ε-cage volume (modeled as $V_{cg} = (V_{cell} - V_{ch})/2$) with P was studied. Both the V_{ch}-P and V_{cg}-P data (Table 4) were fitted with a truncated BM-III equation of state, fixing V_0 to the experimental value at P_0. The refined elastic parameters are: K_{0ch} = 52(3) GPa, K'_{ch} = 1.4(1.0) for the 12mR channel, and K_{0cg} = 53(4) GPa, K'_{cg} = 4(2) for the ε-cage.

High-pressure extraframework behavior

The *Na*1 site, which lies in the ε cage, coordinates the neighboring 6mR's oxygen and two H_2O molecules (ditrigonal bipyramid coordination shell) (Fig. 3). The distortion of this polyhedron is strictly governed by the framework deformation. With increasing pressure, we observe a contraction of the *Na*1-*O*2 and an expansion of the *Na*1-*O*1 bond lengths (Table 4). The two *Na*1-*Ow* distances of the coordination polyhedron are symmetrically independent and both show a shortening with pressure (Table 4).

The sum of the refined site occupancies of the mutually exclusive carbonate groups is lower than 1 (Table 3), reflecting site vacancy. The absence of any superstructure reflections suggests that these vacancies are randomly distributed along the 12mR channels. Three combinations of subsequent

CO_3 groups are possible: *C*1-*C*2 (3.85(7) Å at room-*P*), *C*1-*C*1 and *C*2-*C*2 (both spaced by *c*/2, 2.542(2) Å at room-*P*) (Fig. 4; Table 4).

The *Na*2 site is coordinated by 5 framework oxygen atoms on a side and up to 3 carbonate oxygen atoms on the opposite side (Fig. 3). With increasing pressure, we observe a decrease of the shorter *Na*2-*O*3', *Na*2-*O*4' and *Na*2-*O*1 bond lengths and an expansion of the longer *Na*2-*O*3'' and *Na*2-*O*4'', whereas no significant change occurs for the *Na*2-*Oc* distances (Table 4).

Discussion

Elastic behavior

The refined isothermal bulk modulus at room-*P* (*i.e.* K_{V0} = 45-52 GPa) is similar to that of other microporous materials which share with cancrinite the presence of "6-membered rings" of tetrahedra as "secondary building units" (*sensu* Baerlocher et al. 2007) (Gatta 2008), among those: sodalite (*i.e.* K_{V0} = 51(1) GPa; Hazen and Sharp 1988), levyne (*i.e.* K_{V0} = 56(4) GPa for $P < 1$ GPa, 46(1) GPa for $P > 1$ GPa; Gatta et al. 2005), and chabazite (*i.e.* K_{V0} = 35(5) GPa for $P \leq 1$GPa, 62(1) GPa for $P \geq 1.4$ GPa; Leardini et al. 2010). The stiffer open-framework silicates show bulk moduli of 60-70 GPa (*e.g.* philippsite K_{V0} = 67(2) GPa, Gatta and Lee 2007; gismondine K_{V0} = 63.8(2), Ori et al. 2008), whereas for the softest the range is 18-40 GPa (*e.g.* Na-ZSM-5 K_{V0} = 18.2(6) GPa, Arletti et al. 2011; H-ZSM-5 K_{V0} = 23.7(4) GPa, Quartieri et al. 2011; zeolite-A K_{V0} = 22.1(3), Arletti et al. 2003; heulandite K_{V0} = 27.5(2), Gatta et al. 2003; mordenite K_{V0} = 41(2) GPa, Gatta and Lee 2006).

A subtle change in the elastic behavior of cancrinite appears to occur at $P > 4.6$ GPa (Fig. 5). However, the accuracy and precision of our data, along with the *P*-range investigated, do not allow to have a unique picture of the elastic behavior. In addition, a potential change of the compressional mechanisms at $P > 4.6$ GPa is not supported by the deformation mechanisms deduced on the basis of the H*P* structure refinements, by any change of the symmetry or by any evidence of satellite reflections (Fig. 6, Table 4).

The elastic behavior of the natural cancrinite here investigated differs significantly from that of the isotypic $Na_6Cs_2Ga_6Ge_6O_{24}{\cdot}Ge(OH)_6$. The compressional behavior of the synthetic analogue was fitted with a Murnaghan-type equation of state (Murnaghan 1937) by Gatta and Lee (2008), giving: K_{V0}

289 = 36(2) GPa and K_V' = 9(1) GPa. Possible reasons for the higher compressibility at room-*P*, along with
290 the higher stiffness rate of the synthetic compound, can be found in the compression of the (Ga,Ge)
291 tetrahedra, which is already significant in response to moderate pressure (*i.e.* $P < 5$ GPa) if compared to
292 the almost rigid behavior of the (Si,Al) tetrahedra of the natural sample (Table 4), and in the different
293 nature of the extraframework population.

294

295 *High-pressure framework behavior*

296 The main deformation mechanism in the cancrinite framework in response to the applied pressure is the
297 anti-cooperative rotation of adjacent tetrahedra belonging to the 6mRs⊥[0001]. This mechanism
298 requires that for a given tetrahedron belonging to the A plane which shows a clockwise rotation, the
299 four adjacent vertex-sharing tetrahedra (three on the same A plane and one on the next B plane) will
300 show an anti-clockwise rotation (Fig. 2). The 6mRs⊥[0001] ditrigonalization is the main effect of the
301 anti-cooperative rotation mechanism, leading to the 12mR-channels contraction along the *O*1-*O*1
302 distances (Figs. 2 and 6). The (*O*1-*O*1/*O*3-*O*4) ratio decreases with *P* from 1.038(3) at 0.0001 GPa to
303 0.989(2) at 6.63 GPa (Table 4). The shortest free diameter of the channels (*i.e. O*3-*O*4) is nearly
304 constant up to ~5.3-5.4 GPa and then decreases at higher pressure. On the whole, *a*) the channel *O*1-*O*1
305 shortening coupled with *b*) the 4mR joint-units compression along the *O*3-*O*4 direction and *c*) the
306 6mRs⊥[0001] compression (described by the *O*1-*O*2 shortening, Table 4) are the mechanisms
307 responsible for the *P*-driven contraction on the (0001) plane (Figs. 2 and 6), whereas the compression
308 along the *c* axis is accommodated by *a*) the ε-cage flattening, *b*) the decrease of the (A,B)-planes
309 corrugation and *c*) the ditrigonal distortion of the 6mRs//[0001] windows connecting channels and
310 cages (Figs. 2 and 6; Table 4).

311 The elastic parameters obtained from the compressional behavior of the 12mR-channel and of
312 the ε cage (Table 4) show that these units have similar bulk moduli at room-*P*, but cage becomes stiffer
313 with increasing pressure, likely for the presence of the ···Na-H_2O··· chains as cage-population which
314 can hinder the compression of the cage.

315 The isotypic $Na_6Cs_2Ga_6Ge_6O_{24}{\cdot}Ge(OH)_6$ variant (Gatta and Lee 2008), despite the significant
316 differences in the nature of framework and extraframework population, shows the same *P*-induced
317 main deformation mechanisms found in natural cancrinite. On this basis, we believe that the main

deformation mechanisms here described might be intrinsically governed by the CAN framework topology. As a matter of fact, a comparison with the structural evolution of a natural cancrinite at high-temperature conditions, on the basis of the data reported by Hassan et al. (2006), shows the same deformation mechanisms, but opposite in sign, here observed at high pressure.

High-pressure extraframework behavior

At high pressure, the *Na*1 to framework-oxygen bond lengths variation appears to be the effect of the 6mRs⊥[0001] ditrigonalization, whereas the compression along [0001] governs the bond lengths shortening along the ···Na–H_2O—Na–H_2O··· chains (Fig. 3; Table 4).

Different coordination shells, with maximum coordination number (C.N.) of 8, are possible for the Na/Ca mixed *Na*2 site, due to the different CO_3 ordering but with a fixed coordination with 5 framework oxygen (Fig. 3). At high pressure, the expansion of the longer *Na*2-*O*3'' and *Na*2-*O*4'' bond lengths leads an increasingly weaker interaction with these atoms, suggesting an actual C.N. = 6 at these conditions.

The contraction of the short *C*1-*C*1 and *C*2-*C*2 distances (equal to *c*/2) at high pressure suggests an increasing instability for these stacking configurations in favor of the longer *C*1-*C*2 one (~3.85 Å at room-*P*), if we consider the C-C distance in aragonite (~2.87 Å) as the shortest reported in carbonates (Bonaccorsi and Merlino 2005). However, previous structure refinements of natural cancrinites from X-ray and neutron diffraction data (*e.g.* Ballirano and Maras 2005; Della Ventura et al. 2009, Gatta et al. 2011) showed anisotropic displacement parameters of the CO_3 group significantly elongated along [0001], likely due to a positional disorder aimed to optimize the C-C distances at a local scale toward an energetically less costly configuration.

The role of the extraframework population on the high-pressure structure evolution of natural cancrinite appears to be only secondary, suggesting that the *P*-induced structure response is mainly governed by the framework deformation mechanisms, which, in turn, are likely controlled by the CAN topology.

Acknowledgments

Giancarlo Della Ventura and Fabio Bellatreccia (Università Roma Tre) are thanked for the crystals of cancrinite from Cameroun. Giorgio Pafundi and Bruno Pafundi are thanked for the set-up of the H*P*-lab in Milan. The reviewers Simona Quartieri and Ronald Miletich, the Technical Editor (Ron Peterson) and the Associate Editor (Alexandra Friedrich) are thanked. This work was funded by the Italian Ministry of University and Research, MIUR-Project: 2008SPZ743.

References

Angel, R.J. (2000) Equations of state. In R.M. Hazen and R.T. Downs, eds., High-temperature and high-pressure crystal chemistry, vol. 41, pp. 35–60. Reviews in Mineralogy and Geochemistry, Mineralogical Society of America and the Geochemical Society, Chantilly, Virginia.

Angel RJ (2004) Absorption corrections for diamond-anvil pressure cells implemented in a software package Absorb-6.0. Journal of Applied Crystallography, 37, 486-492.

Angel, R.J., Allan, D.R., Miletich, R. and Finger, L.W. (1997) The use of quartz as internal pressure calibrant in high-pressure crystallography. Journal of Applied Crystallography, 30, 461–466.

Angel, R.J., Bujak, M., Zhao, J., Gatta, G.D. and Jacobsen, S.J. (2007) Effective hydrostatic limits of pressure media for high-pressure crystallographic studies. Journal of Applied Crystallography, 40, 26-32.

Arletti, R., Ferro, O., Quartieri, S., Sani, A., Tabacchi, G., and Vezzalini, G. (2003) Structural deformation mechanisms of zeolites under pressure. American Mineralogist, 88, 1416-1422.

Arletti, R., Vezzalini, G., Morsli, A., Di Renzo, F., Dmitriev, V. and Quartieri, S. (2011) Elastic behavior of MFI-type zeolites: 1- Compressibility of Na-ZSM-5 in penetrating and non-penetrating media. Microporous and Mesoporous Materials, 142, 696-707.

Baerlocher, C., McCusker, L.B. and Olson, D.H. (2007) Atlas of zeolite framework types (sixth edition), 84 p., Elsevier, Amsterdam.

Ballirano, P. and Maras, A. (2005) The crystal structure of a "disordered" cancrinite. European Journal of Mineralogy, 16, 135–141.

Barnes, M.C., Addai-Mensah, J. and Gerson, A.R. (1999) The mechanism of the sodalite-to-cancrinite phase transformation in synthetic spent Bayer liquor. Microporous and Mesoporous Materials, 31, 287–302.

Bickmore, B.R., Nagy, K.L., Young, J.S. and Drexler, J.W. (2001) Nitrate-Cancrinite Precipitation on Quartz Sand in Simulated Hanford Tank Solutions. Environmental Science and Technology, 35, 4481–4486.

Birch, F. (1947) Finite elastic strain of cubic crystals. Physical Review, 71, 809-824.

Bonaccorsi, E. and Merlino, S. (2005) Modular microporous minerals: Cancrinite-Davyne group and C-S-H phases. In G. Ferraris and S. Merlino, Eds., Micro- and mesoporous mineral phases, vol. 57, p. 241–290. Reviews in Mineralogy and Geochemistry, Mineralogical Society of America and the Geochemical Society, Chantilly, Virginia.

Bonaccorsi, E., Ballirano, P., Cámara, F. (2012) The crystal structure of sacrofanite, the 74 Å phase of the cancrinite–sodalite supergroup , Microporous and Mesoporous Materials, 147, 318-326.

Bresciani-Pahor, N., Calligaris, M., Nardin, G. and Randaccio, L. (1982) Structure of a Basic Cancrinite. Acta Crystallographica, B38, 893–895.

Buck, E.C. and McNamara, B.K. (2004) Precipitation of Nitrate-Cancrinite in Hanford Tank Sludge. Environmental Science and Technology, 38, 4432–4438.

Brigatti, M.F. and Guggenheim, S. (2002) Mica crystal chemistry and the influence of pressure, temperature, and solid solution on atomistic models. In A. Mottana, F.P. Sassi, J.B. Thompson Jr. and S. Guggenheim, eds, Micas: crystal chemistry and metamorphic petrology, vol. 46, pp. 1–98. Reviews in Mineralogy and Geochemistry, Mineralogical Society of America and the Geochemical Society, Chantilly, Virginia.

Brown, W.L. and Cesbron, F. (1973) Sur les surstructures des cancrinites. Comptes Rendus de l'Academie de Sciences, 276(Aer. D), 1–4.

Buck, E.C. and McNamara, B.K. (2004) Precipitation of Nitrate-Cancrinite in Hanford Tank Sludge. Environmental Science and Technology, 38, 4432–4438.

Buhl, J.C., Stief, F., Fechtelkord, M., Gesing, T.M., Taphorn, U. and Taake, C. (2000) Synthesis, X-ray diffraction and MAS NMR characteristics of nitrate cancrinite $Na_{7.6}[AlSiO_4]_6(NO_3)_{1.6}(H_2O)_2$. Journal of Alloys and Compounds, 305, 93–102.

Cámara, F., Bellatreccia, F., Della Ventura, G. and Mottana, A. (2005) Farneseite, a new mineral of the cancrinite-sodalite group with a 14 layer stacking sequence: occurrence and crystal structure. European Journal of Mineralogy, 17, 839–846.

Cámara, F., Bellatreccia, F., Della Ventura, G., Mottana, A., Bindi, L., Gunter, M.E. and Sebastiani, M. (2010) Fantappièite, a new mineral of the cancrinite-sodalite group with a 33-layer stacking sequence: Occurrence and crystal structure. American Mineralogist, 95, 472–480.

Della Ventura, G., Gatta, G.D., Redhammer, G.J., Bellatreccia, F., Loose, A. and Parodi, G.C. (2009) Single-crystal polarized FTIR spectroscopy and neutron diffraction refinement of cancrinite. Physics and Chemistry of Minerals, 36, 193–206.

Fechtelkord, M., Stief, F. and Buhl, J.C. (2001) Sodium cation dynamics in nitrate cancrinite: A low and high temperature ^{23}Na and ^{1}H MAS NMR study and high temperature Rietveld structure refinement. American Mineralogist, 86, 165–175.

Foit, F.F. Jr., Peacor, D.R and Heinrich, E.W.M. (1973) Cancrinite with a new superstructure from Bancroft, Ontario. Canadian Mineralogist, 11, 940–951.

Gatta, G.D. (2008) Does porous mean soft? On the elastic behaviour and structural evolution of zeolites under pressure. Zeitschrift fur Kristallografie, 223, 160–170.

Gatta, G.D., Comodi, P., and Zanazzi, P.F. (2003): New insights on high-pressure behaviour of microporous materials from X-ray single crystal data. Microporous and Mesoporous Materials, 61, 105-111.

Gatta, G.D. and Lee, Y. (2006) On the elastic behavior of zeolite mordenite. A synchotron powder diffraction study. Physics and Chemistry of Minerals, 32, 726–732.

Gatta, G.D. and Lee, Y. (2007) Anisotropic elastic behavior and structural evolution of zeolite phillipsite at high-pressure: a synchrotron powder diffraction study. Microporous and Mesoporous Materials, 135, 239–250.

Gatta, G.D. and Lee, Y. (2008) Pressure-induced structural evolution and elastic behaviour of $Na_6Cs_2Ga_6Ge_6O_{24}{\cdot}Ge(OH)_6$ variant of cancrinite: A synchrotron powder diffraction study. Microporous and Mesoporous Materials, 116, 51–58.

Gatta, G.D., Comodi, P., Zanazzi, P.F. and Boffa Ballaran, T. (2005) Anomalous elastic behavior and high-pressure structural evolution of zeolite levyne. American Mineralogist, 90, 645–652.

Gatta, G.D., Lotti, P., Kahlenberg, V. and Haefeker, U. (2012) On the low-temperature behavior of cancrinite: an *in-situ* single-crystal X-ray diffraction study. Mineralogical Magazine (*in press*).

Gerson, A.R. and Zheng, K. (1997) Bayer process plant scale: transformation of sodalite to cancrinite. Journal of Crystal Growth, 171, 209–218.

Grundy, H.D. and Hassan, I. (1982) The crystal structure of a carbonate-rich cancrinite. Canadian Mineralogist, 20, 239–251.

Hassan, I. and Buseck, P.R. (1992) The origin of the superstructure and modulations in cancrinite. Canadian Mineralogist, 30, 49–59.

Hassan, I. and Grundy, H.D. (1984) The character of the cancrinite-vishnevite solid solution series. The Canadian Mineralogist, 22, 333–340.

Hassan, I. and Grundy, H.D. (1991) The crystal structure of basic cancrinite, ideally $Na_8[Al_6Si_6O_{24}](OH)_2{\cdot}3H_2O$. Canadian Mineralogist, 29, 377–383.

Hassan, I., Antao, S.M. and Parise, J.B. (2006) Cancrinite: Crystal structure, phase transitions, and dehydration behavior with temperature. American Mineralogist, 91, 1117-1124.

Hazen, R.M. and Sharp, Z.D. (1988) Compressibility of sodalite and scapolite. American Mineralogist, 73, 1120–1122.

449 Isupova, D., Ida, A., Kihara, K., Morishita, T. and Bulka, G. (2010) Asymmetric thermal vibrations of
450 atoms and pyroelectricity in cancrinite. Journal of Mineralogical and Petrological Sciences, 105, 29–41.

451 Jarchow, O. (1965) Atomanordnung und strukturverfeinerung von Cancrinit. Zeitschrift fur
452 Kristallografie, 122, 407–422

453 Leardini, L., Quartieri, S. and Vezzalini, G. (2010) Compressibility of microporous materials with
454 CHA topology: 1. Natural chabazite and SAPO-34. Microporous and Mesoporous Materials, 127, 219-
455 227.

456 Mao, H.K., Xu, J. and Bell, P.M. (1986) Calibration of the ruby pressure gauge to 800 kbar under
457 quasi-hydrostatic conditions. Journal of Geophysical Research, 91, 4673-4676.

458 Miletich, R, Allan, D.R. and Kuhs, W.F. (2000) High-pressure single-crystal techniques. In R.M.
459 Hazen and R.T. Downs, eds., High-temperature and high-pressure crystal chemistry, vol. 41, pp. 445–
460 519. Reviews in Mineralogy and Geochemistry, Mineralogical Society of America and the
461 Geochemical Society, Chantilly, Virginia.

462 Murnaghan, F.D. (1937) Finite deformations of an elastic solid. American Journal of Mathematic, 49,
463 235-260.

464 Oxford Diffraction (2010) Oxford Diffraction Ltd., Xcalibur CCD system, CrysAlis Software system.

465 Ori, S., Quartieri, S., Vezzalini, G., and Dmitriev, V. (2008) Pressure-induced over-hydration and water
466 ordering in gismondine: A synchrotron powder diffraction study. American Mineralogist, 93, 1393–
467 1403.

468 Pauling, L. (1930) The structure of some sodium and calcium aluminosilicates. Proceedings of the
469 National Academy of Sciences, 16, 453–459.

470 Poborchii, V.V. (1994) Structure of one-dimensional selenium chains in zeolite channels by polarized
471 Raman scattering. Journal of Physics and Chemistry of Solids, 55, 737–774.

472 Poborchii, V.V., Lindner, G.G. and Sato, M. (2002) Selenium dimers and linear chains in one-
473 dimensional cancrinite nanochannels: Structure, dynamics, and optical properties. Journal of Chemical
474 Physics, 116, 2609–2617.

475 Quartieri, S., Montagna, G., Arletti, R. and Vezzalini, G. (2011) Elastic behavior of MFI-type zeolites:
476 Compressibility of H-ZSM-5 in pentrating and non-penetrating media. Journal of Solid State
477 Chemistry, 184, 1505-1516.

478 Rastvetaeva, R., Pekov, I., Chukanov, N., Rozenberg, K. and Olysych, L. (2007) Crystal structures of
479 low-symmetry cancrinite and cancrisilite varieties. Crystallography Reports, 52, 811–818.

480 Sheldrick, G.M. (1997) SHELX-97 – A program for crystal structure refinement. University of
481 Goettingen, Germany.

482 Wilson, A.J.C. and Prince, E. (1999) International Tables for Crystallography Vol. C, Mathematical,
483 physical anc chemical tables (third edition), 578 p., Kluwer, Dordrecht.

484 Zhao, H., Deng, Y., Harsh, J.B., Flury, M. and Boyle, J.S. (2004) Alteration of kaolinite to cancrinite
485 and sodalite by simulated Hanford tank waste and its impact on Cesium retention. Clays and Clay
486 Minerals, 52, 1–13.

487

Figure 1. (*Left side*) The building scheme of the CAN framework: planes of 6-membered rings of tetrahedra perpendicular to [0001] are stacked according to an ABAB close-packing sequence. (*Right side*) A column, parallel to [0001], of base-sharing ε cages. Three *double zigzag chains* run along the column.

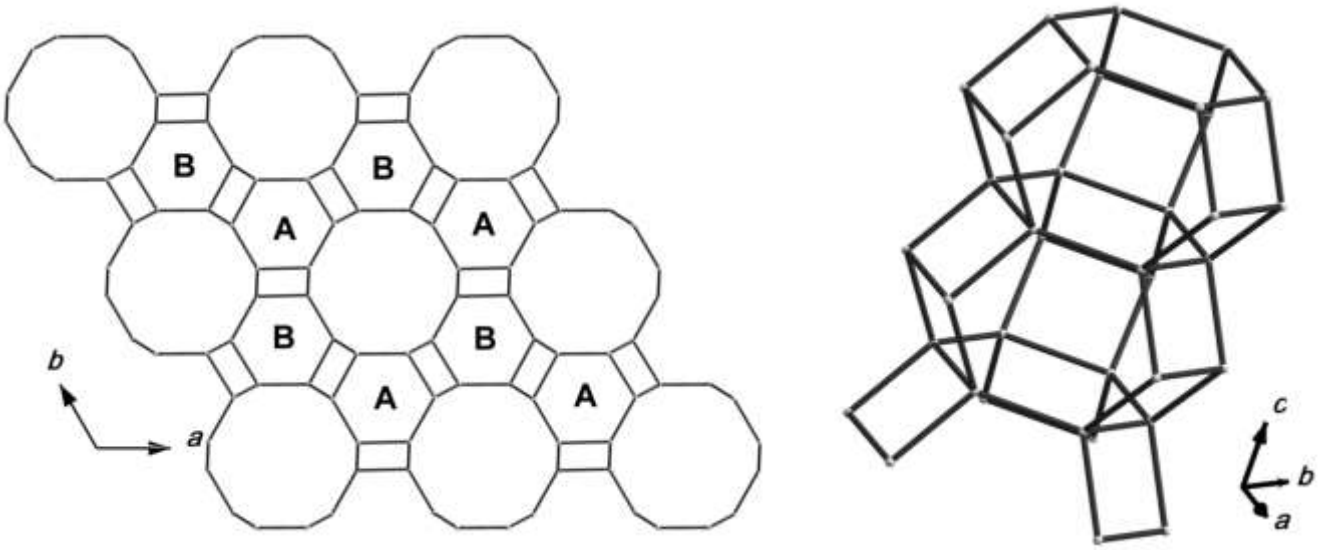

Figure 2. (A) The cancrinite framework viewed down [0001]. (B) The ε cage, with a view of the κ angle (O2-O2-O2) and of the 6mR//[0001] window's diameters. (C and D) The 6mR⊥[0001] at room-*P* (C) and at 6.63 GPa (D). *P*-induced anti-cooperative rotation of adjacent tetrahedra (ditrigonalization) is shown.

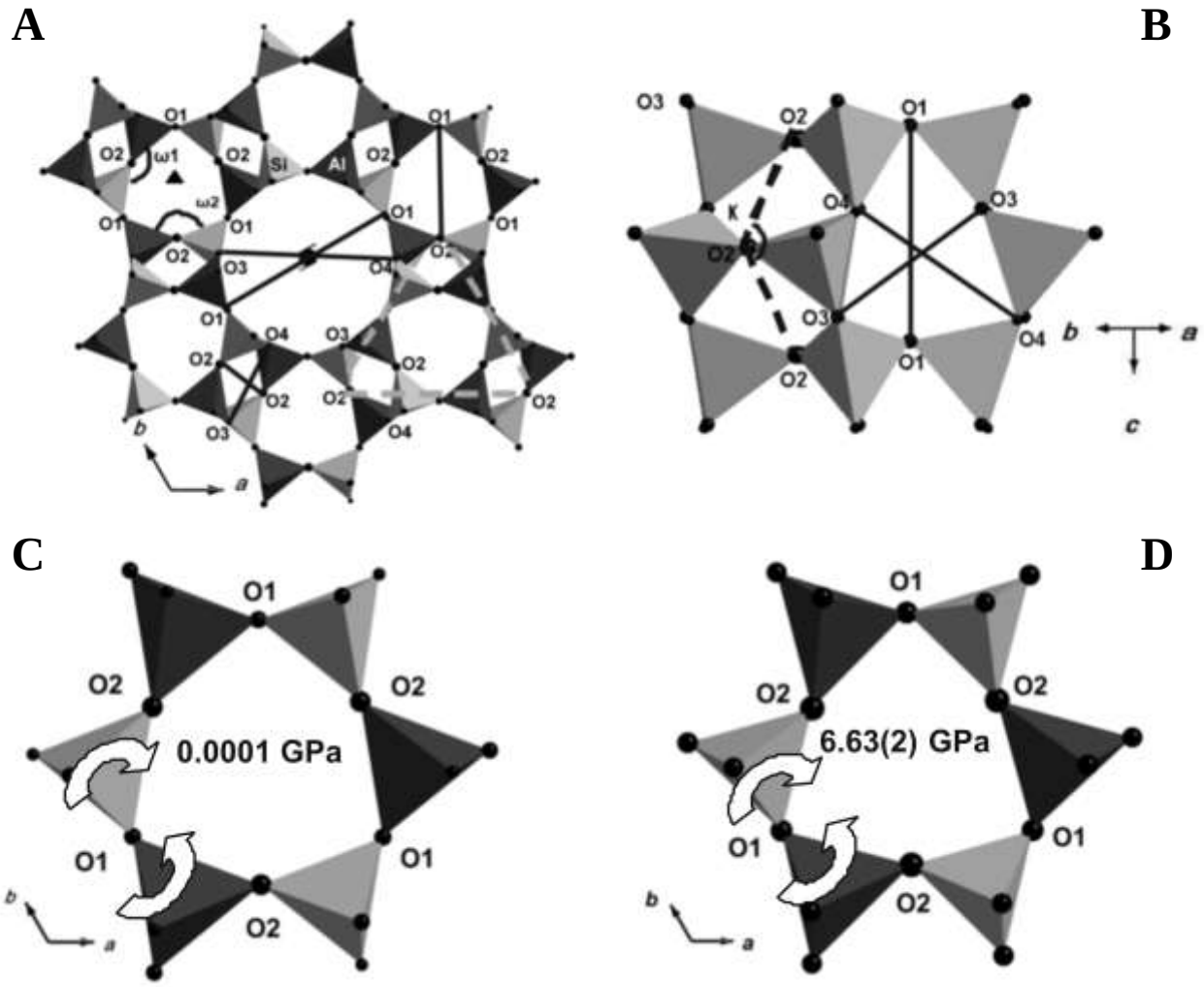

Figure 3. (*Left side*) The coordination shell of the Na1 site. Dashed lines represent mutually exclusive Na-Ow bond lengths. (*Right side*) The coordination shell of the Na2 site (*i.e.* 5 framework oxygen on a side and up to three carbonate oxygen on the opposite side, maximum C.N. = 8).

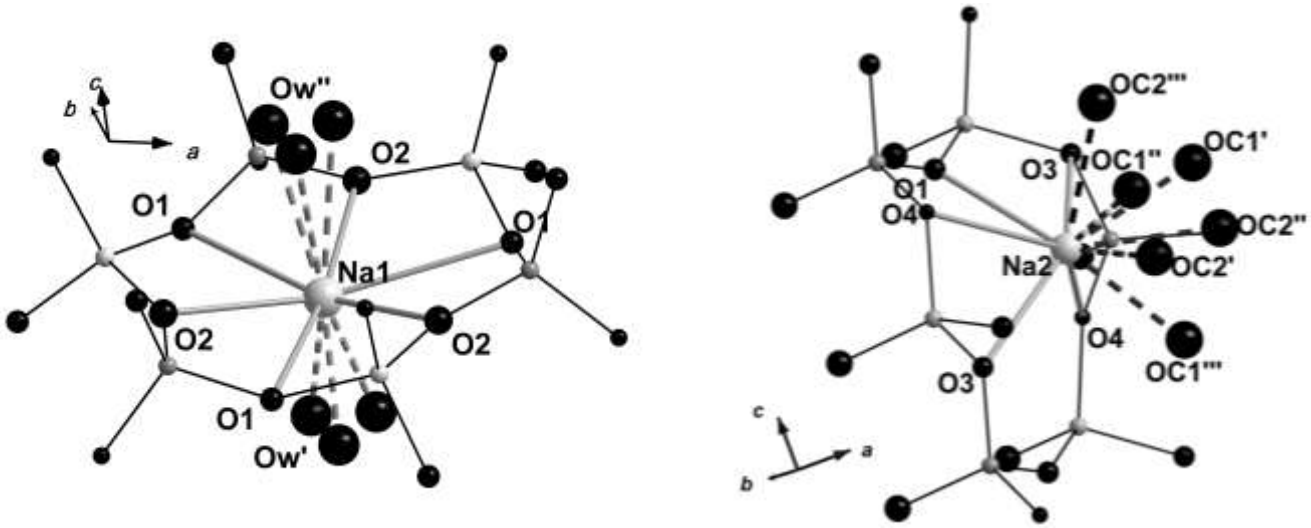

Figure 4. The extraframework population of the 12mR channel, with the Na2 site close to the wall and the carbonate anions lying at the center. Different stacking sequences of the CO_3^{2-} groups and their vacancies are possible.

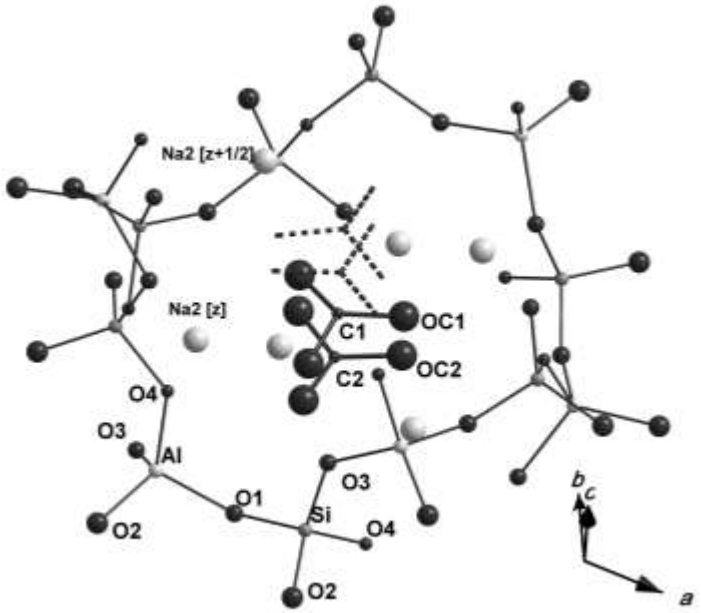

Figure 5. Variation of the unit-cell parameters of cancrinite with pressure and Eulerian finite strain *vs* normalized stress plot (*fe*-*Fe* plot). For the unit-cell parameters *vs. P* plots, the dotted lines represent the axial and volume BM-EoS fits between 0.0001 and 6.63 GPa, whereas the solid lines represents the BM-EoS fit between 0.0001- 4.62 GPa and 5.00-6.63 GPa, respectively (see text for further details). The *e.s.ds* are of the same size of the symbols.

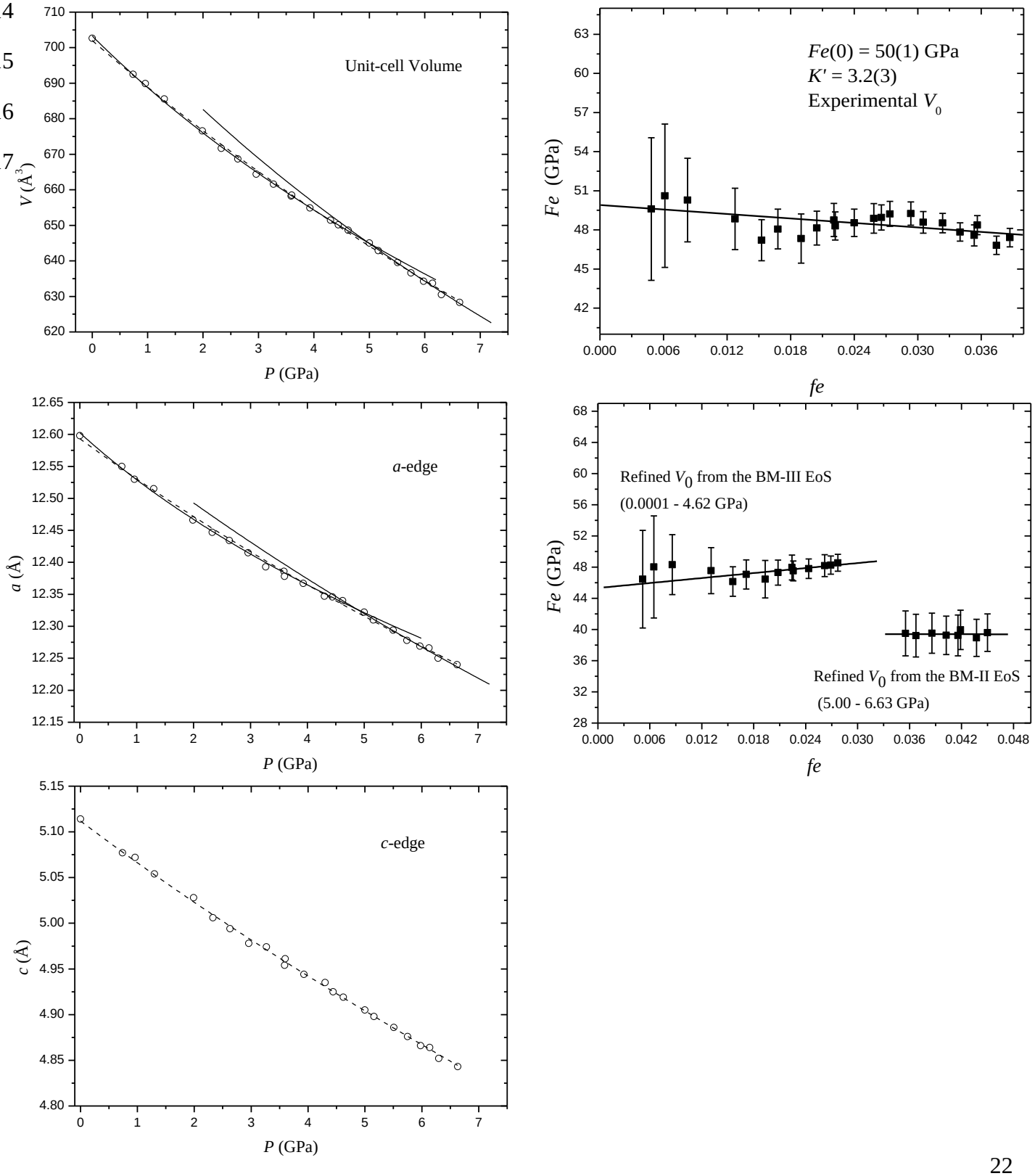

Figure 6. Evolution with *P* of: (A) the ditrigonal rotation angle α of the 6mR⊥[0001] unit, (B) the O3-O4 diameter of the 4mR unit, (C) the O1-O1 diameter of the 12mR unit, and (D) the κ angle (O2-O2-O2) of the ε cage. The weighted linear fits through the data points are shown.

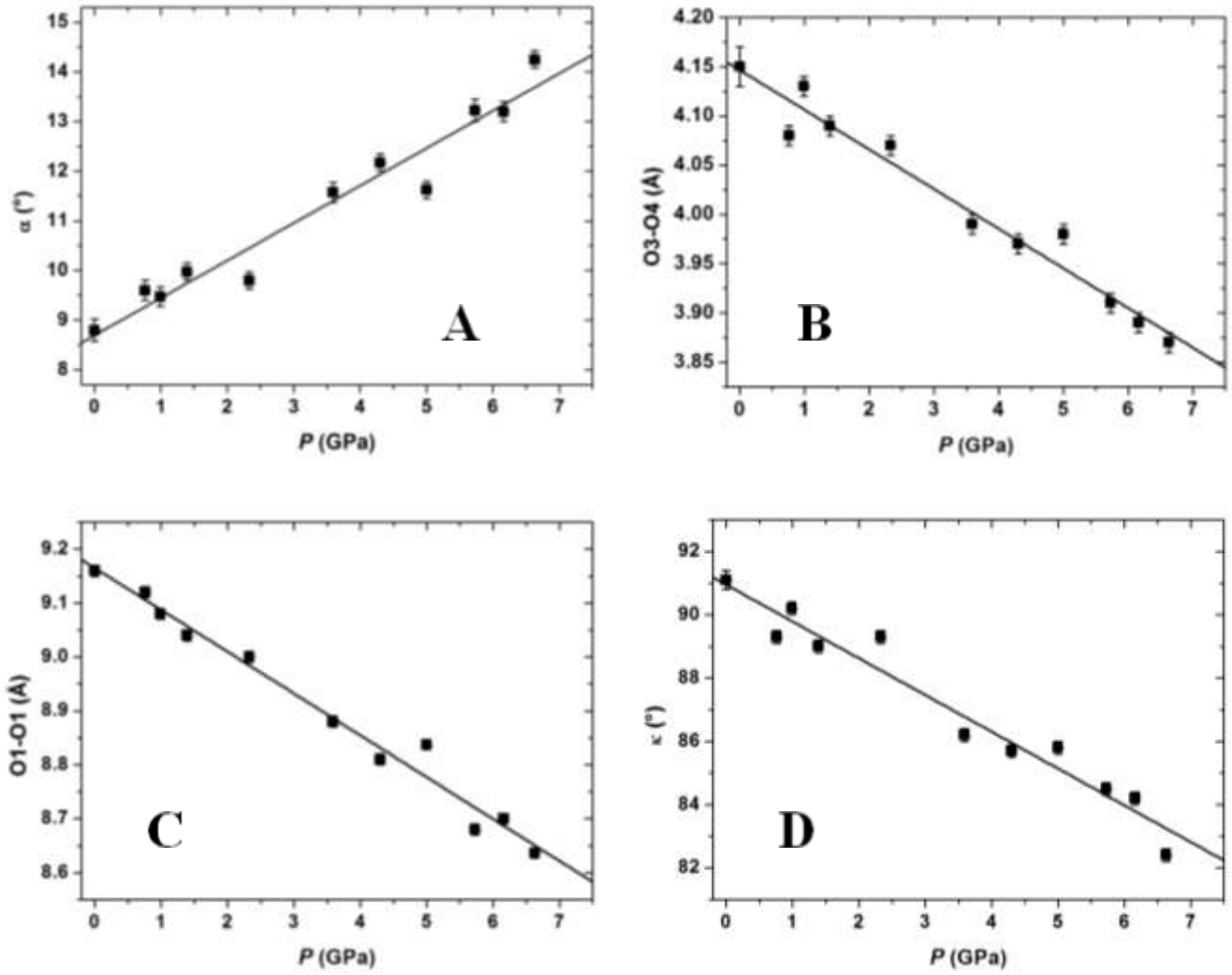

528 Table 1. Details of the data collection strategy and structure refinement of cancrinite at different pressures.

529

530

P (GPa)	0.0001	0.0001*	0.76(2)	0.99(2)	1.39(2)	2.33(2)	3.59(2)	4.30(3)	5.00(2)	5.73(3)	6.16(2)	6.63(3)
X-ray radiation	Mo-*K*α	Mo-*K*α	Mo-*K*α	Mo-*K*α	Mo-*K*α	Mo-*K*α	Mo-*K*α	Mo-*K*α	Mo-*K*α	Mo-*K*α	Mo-*K*α	Mo-*K*α
Scan width (°/frame)	1	0.5	0.5	0.5	0.5	0.5	0.5	0.5	0.5	0.5	0.5	0.5
a (Å)	12.5976(6)	12.620(9)	12.580(9)	12.530(9)	12.514(9)	12.447(5)	12.386(3)	12.347(6)	12.322(4)	12.278(2)	12.266(3)	12.240(4)
c (Å)	5.1168(2)	5.083(4)	5.058(3)	5.072(5)	5.034(2)	5.006(2)	4.954(2)	4.935(3)	4.905(2)	4.876(1)	4.864(2)	4.843(2)
Maximum 2θ (°)	69.96	60.91	64.02	64.05	64.05	64.05	63.42	63.64	63.96	63.66	64.00	63.85
Measured reflections	19,933	1,545	1,858	1,932	2,034	1,838	1,937	2,238	2,019	2,000	2,111	1,945
Unique reflections	1,980	685	789	769	771	722	728	834	780	752	799	704
Unique reflections with $F_0 > 4\sigma(F_0)$	1,092	327	374	396	356	343	325	402	350	337	373	327
R_{int}	0.0581	0.1068	0.0958	0.1177	0.0936	0.0964	0.1088	0.0961	0.0900	0.0972	0.0884	0.0995
N. of refined parameters	87	45	45	45	45	45	45	45	45	45	45	45
R_1, $F_0 > 4\sigma(F_0)$	0.0560	0.0833	0.0888	0.0777	0.0656	0.0549	0.0634	0.0696	0.0606	0.0733	0.0830	0.0694
wR^2	0.0634	0.0925	0.1025	0.1192	0.0946	0.0775	0.0890	0.0958	0.0855	0.1045	0.0958	0.0881
GooF	1.073	1.096	1.036	1.117	1.095	1.285	1.098	1.079	1.080	1.062	1.029	1.024
Residuals (e^-/ Å^3)	+0.77/	+0.71/	+0.65/	+0.66/	+0.70/	+0.77/	+0.66/	+0.60/	+0.61/	+0.79/	+0.76/	+0.89/
	-0.55	-0.85	-0.74	-0.72	-0.73	-0.51	-0.69	-0.87	-0.63	-0.96	-0.80	-0.72

* With the crystal in the DAC without any *P*-medium. At any pressure: ω/φ scan type, 60 s exposure time, $P6_3$ space group.

$R_{int} = \Sigma \mid F_{obs}^2 - F_{obs}^2(mean) \mid / \Sigma [F_{obs}^2]$; $R_1 = \Sigma(|F_{obs}| - |F_{calc}|)/\Sigma|F_{obs}|$; $wR_2 = [\Sigma[w(F^2_{obs} - F^2_{calc})^2]/\Sigma[w(F^2_{obs})^2]]^{0.5}$, $w = 1/ [\sigma^2(F_{obs}^2) + (0.01*P)^2]$, $P = (\text{Max} (F_{obs}^2, 0) + 2*F_{calc}^2)/3$

Table 2. Unit-cell parameters of cancrinite at different pressures measured using a KUMA diffractometer.

P (GPa)	*a* (Å)	*c* (Å)	*V* (Å^3)
0.0001*	12.598(8)	5.114(4)	702.6(8)
0.74(2)	12.550(7)	5.077(3)	692.5(7)
0.96(2)	12.530(9)	5.072(5)	690.0(9)
1.30(2)	12.515(6)	5.054(3)	685.6(6)
1.99(2)	12.466(8)	5.028(4)	676.6(8)
2.33(2)	12.447(5)	5.006(2)	671.7(5)
2.63(2)	12.434(6)	4.994(2)	668.7(5)
2.96(2)	12.415(7)	4.978(7)	664.0(9)
3.27(2)	12.393(5)	4.974(3)	661.6(5)
3.59(2)	12.386(3)	4.954(2)	658.3(3)
3.60(2)	12.378(6)	4.961(3)	658.5(6)
3.93(2)	12.367(4)	4.944(2)	654.9(4)
4.30(3)	12.347(6)	4.935(3)	651.5(6)
4.44(2)	12.346(4)	4.925(2)	650.1(4)
4.62(3)	12.340(3)	4.919(2)	648.6(3)
5.00(2)	12.322(4)	4.905(2)	645.0(4)
5.16(2)	12.310(3)	4.898(2)	642.9(3)
5.51(2)	12.294(2)	4.886(1)	639.6(2)
5.75(2)	12.278(2)	4.876(1)	636.6(2)
5.98(2)	12.269(5)	4.866(3)	634.2(5)
6.14(2)	12.266(3)	4.864(2)	633.7(3)
6.30(3)	12.250(3)	4.852(2)	630.5(3)
6.63(3)	12.240(4)	4.843(2)	628.3(4)

* With the crystal in the DAC without any *P*-medium.
Note: Unit-cell parameters measured with a KUMA point-detector diffractometer.

Table 3. Atomic fractional coordinates, site occupancy factors (s.o.f.), and thermal displacement parameters ($Å^2$) at different pressures.

Sites occupancies at P_0-AIR					
Site	s.o.f.	Site	s.o.f.	Site	s.o.f.
Si	1.0	O4	1.0	Oc1	0.421(7)
Al	1.0	Na1	0.960(9)	C2	0.459(6)
O1	1.0	Na2(Na)	0.854(6)	Oc2	0.459(6)
O2	1.0	Na2(Ca)	0.146(6)	Ow	1.0
O3	1.0	C1	0.421(7)		
Site fractional coordinates and displacement parameters					
P (GPa)	Site	x	y	z	U_{iso}/ U_{eq}
0.0001	Si	0.08267(7)	0.41096(7)	0.7338(2)	0.0090(2)
(P_0-AIR)	Al	0.33709(7)	0.41224(7)	0.7342(2)	0.0087(2)
	O1	0.2014(2)	0.4043(2)	0.6419(4)	0.0155(5)
	O2	0.1145(2)	0.5507(2)	0.7109(5)	0.0198(5)
	O3	0.0443(2)	0.3588(2)	0.0276(4)	0.0164(6)
	O4	0.3212(2)	0.3508(2)	0.0442(4)	0.0148(6)
	Na1	2/3	1/3	0.1159(5)	0.0294(9)
	Na2	0.8742(1)	0.7516(1)	0.7764(2)	0.0287(5)
	C1	0	0	0.914(4)	0.048(6)
	OC1	0.0562(7)	0.1184(4)	0.888(2)	0.052(3)
	C2	0	0	0.649(3)	0.021(4)
	OC2	0.0639(5)	0.1196(3)	0.664(1)	0.030(2)
	Ow	0.315(1)	0.6171(6)	0.171(1)	0.048(3)
0.0001	Si	0.0824(3)	0.4106(3)	0.7244(8)	0.0082(9)
(P_0-DAC)	Al	0.3372(3)	0.4126(3)	0.7231(9)	0.0087(9)
	O1	0.2007(7)	0.4027(7)	0.634(1)	0.013(2)
	O2	0.1140(6)	0.5520(7)	0.698(2)	0.019(2)
	O3	0.0462(8)	0.3590(8)	0.020(2)	0.012(3)
	O4	0.3199(8)	0.3517(7)	0.036(1)	0.007(2)
	Na1	2/3	1/3	0.108(2)	0.038(3)
	Na2	0.8746(4)	0.7519(4)	0.7673(5)	0.027(1)
	C1	0	0	0.91(1)	0.006(9)
	OC1	0.058(2)	0.1182(8)	0.881(6)	0.038(5)
	C2	0	0	0.652(9)	0.006(9)
	OC2	0.062(2)	0.1190(5)	0.662(4)	0.038(5)
	Ow	0.316(4)	0.617(2)	0.173(4)	0.039(9)
0.76(2)	Si	0.0828(3)	0.4112(3)	0.7347(7)	0.0095(7)
	Al	0.3373(3)	0.4126(3)	0.7348(9)	0.0111(8)
	O1	0.2009(7)	0.4022(7)	0.639(1)	0.015(2)
	O2	0.1175(6)	0.5542(6)	0.704(1)	0.019(2)
	O3	0.0491(7)	0.3632(7)	0.034(2)	0.014(2)
	O4	0.3212(7)	0.3540(7)	0.048(2)	0.010(2)
	Na1	2/3	1/3	0.112(1)	0.041(3)
	Na2	0.8754(4)	0.7517(4)	0.7779(6)	0.032(1)
	C1	0	0	0.90(2)	0.04(1)
	OC1	0.061(2)	0.1190(8)	0.883(6)	0.048(5)

	C2	0	0	0.672(4)	0.04(1)
	OC2	0.062(2)	0.1193(5)	0.672(4)	0.048(5)
	Ow	0.306(4)	0.613(2)	0.181(4)	0.054(9)
0.99(2)	Si	0.0826(3)	0.4108(3)	0.7376(6)	0.0139(7)
	Al	0.3374(2)	0.4121(3)	0.7389(7)	0.0133(8)
	O1	0.2000(7)	0.4017(7)	0.644(1)	0.020(2)
	O2	0.1163(6)	0.5513(6)	0.707(1)	0.020(2)
	O3	0.0457(7)	0.3588(7)	0.034(1)	0.015(2)
	O4	0.3191(7)	0.3512(7)	0.053(1)	0.017(2)
	Na1	2/3	1/3	0.115(1)	0.036(2)
	Na2	0.8733(3)	0.7497(4)	0.7820(6)	0.032(1)
	C1	0	0	0.91(1)	0.05(1)
	OC1	0.056(3)	0.119(1)	0.864(7)	0.069(6)
	C2	0	0	0.66(1)	0.05(1)
	OC2	0.063(2)	0.1200(5)	0.657(5)	0.069(6)
	Ow	0.309(3)	0.608(2)	0.173(4)	0.05(1)
1.39(2)	Si	0.0829(2)	0.4109(2)	0.7342(6)	0.0105(7)
	Al	0.3372(2)	0.4121(3)	0.7356(7)	0.0112(7)
	O1	0.2004(6)	0.4006(7)	0.635(1)	0.017(2)
	O2	0.1180(5)	0.5533(6)	0.702(1)	0.022(2)
	O3	0.0484(6)	0.3620(6)	0.035(1)	0.013(2)
	O4	0.3183(6)	0.3535(6)	0.054(1)	0.015(2)
	Na1	2/3	1/3	0.110(1)	0.040(2)
	Na2	0.8743(3)	0.7508(3)	0.7784(5)	0.032(1)
	C1	0	0	0.90(1)	0.028(9)
	OC1	0.058(2)	0.1200(6)	0.886(6)	0.052(5)
	C2	0	0	0.671(4)	0.028(9)
	OC2	0.063(2)	0.1203(5)	0.671(4)	0.052(5)
	Ow	0.305(3)	0.614(2)	0.178(4)	0.056(8)
2.33(2)	Si	0.0829(2)	0.4111(2)	0.7340(7)	0.0103(6)
	Al	0.3369(2)	0.4123(3)	0.7357(8)	0.0092(7)
	O1	0.2004(6)	0.4010(7)	0.634(1)	0.016(2)
	O2	0.1174(5)	0.5525(5)	0.699(1)	0.021(2)
	O3	0.0494(6)	0.3629(7)	0.0390(1)	0.014(2)
	O4	0.3181(6)	0.3529(6)	0.058(1)	0.016(2)
	Na1	2/3	1/3	0.107(1)	0.042(2)
	Na2	0.8749(3)	0.7524(3)	0.7792(5)	0.0283(9)
	C1	0	0	0.90(1)	0.032(8)
	OC1	0.052(2)	0.1193(7)	0.870(5)	0.053(5)
	C2	0	0	0.655(9)	0.032(8)
	OC2	0.067(2)	0.1198(6)	0.672(3)	0.053(5)
	Ow	0.319(4)	0.617(2)	0.176(3)	0.047(6)
3.59(2)	Si	0.0831(3)	0.4112(3)	0.7360(7)	0.0101(7)
	Al	0.3367(3)	0.4124(3)	0.7393(8)	0.0105(7)
	O1	0.1988(7)	0.3977(7)	0.631(1)	0.017(2)
	O2	0.1232(6)	0.5556(6)	0.697(1)	0.020(2)
	O3	0.0529(7)	0.3664(6)	0.047(1)	0.014(2)
	O4	0.3189(6)	0.3581(6)	0.062(1)	0.015(2)

	Na1	2/3	1/3	0.100(1)	0.038(2)
	Na2	0.8755(3)	0.7523(3)	0.7785(6)	0.028(1)
	C1	0	0	0.91(1)	0.05(1)
	OC1	0.066(3)	0.119(1)	0.860(5)	0.054(5)
	C2	0	0	0.686(9)	0.05(1)
	OC2	0.057(2)	0.1210(6)	0.664(4)	0.054(5)
	Ow	0.308(3)	0.615(2)	0.159(3)	0.031(7)
4.30(3)	Si	0.0835(2)	0.4111(3)	0.7345(7)	0.0120(6)
	Al	0.3369(2)	0.4126(3)	0.7366(8)	0.0125(7)
	O1	0.1981(6)	0.3957(7)	0.628(1)	0.019(2)
	O2	0.1243(5)	0.5566(6)	0.691(1)	0.020(2)
	O3	0.0539(6)	0.3675(6)	0.046(1)	0.015(2)
	O4	0.3181(6)	0.3579(6)	0.063(1)	0.017(2)
	Na1	2/3	1/3	0.095(1)	0.040(2)
	Na2	0.8754(3)	0.7523(3)	0.7756(6)	0.0291(9)
	C1	0	0	0.90(1)	0.026(8)
	OC1	0.055(2)	0.1204(9)	0.867(5)	0.053(5)
	C2	0	0	0.682(7)	0.026(8)
	OC2	0.067(2)	0.1216(5)	0.669(4)	0.053(5)
	Ow	0.311(3)	0.617(2)	0.155(2)	0.031(6)
5.00(2)	Si	0.0841(2)	0.4116(2)	0.7369(7)	0.0127(6)
	Al	0.3372(2)	0.4131(3)	0.7384(8)	0.0123(7)
	O1	0.1984(6)	0.3978(6)	0.626(1)	0.016(2)
	O2	0.1235(6)	0.5554(6)	0.691(1)	0.024(2)
	O3	0.0546(7)	0.3666(6)	0.048(1)	0.014(2)
	O4	0.3182(6)	0.3584(6)	0.067(1)	0.017(2)
	Na1	2/3	1/3	0.094(1)	0.039(2)
	Na2	0.8757(3)	0.7527(3)	0.7795(6)	0.0276(9)
	C1	0	0	0.918(9)	0.025(8)
	OC1	0.054(2)	0.118(1)	0.857(5)	0.050(4)
	C2	0	0	0.659(8)	0.025(8)
	OC2	0.065(2)	0.1218(5)	0.665(4)	0.050(4)
	Ow	0.314(3)	0.614(2)	0.151(3)	0.045(8)
5.73(3)	Si	0.0839(3)	0.4118(3)	0.7377(8)	0.0123(7)
	Al	0.3377(3)	0.4137(3)	0.7415(9)	0.0131(8)
	O1	0.1955(7)	0.3916(8)	0.625(1)	0.020(2)
	O2	0.1259(7)	0.5560(7)	0.686(1)	0.027(2)
	O3	0.0574(8)	0.3702(6)	0.058(1)	0.014(2)
	O4	0.3196(7)	0.3617(7)	0.072(2)	0.017(2)
	Na1	2/3	1/3	0.085(2)	0.049(3)
	Na2	0.8760(4)	0.7531(4)	0.7764(7)	0.030(1)
	C1	0	0	0.90(1)	0.024(9)
	OC1	0.060(3)	0.121(1)	0.855(6)	0.047(5)
	C2	0	0	0.67(1)	0.024(9)
	OC2	0.064(2)	0.1226(5)	0.668(4)	0.047(5)
	Ow	0.308(4)	0.614(2)	0.151(3)	0.048(9)
6.16(2)	Si	0.0842(3)	0.4119(3)	0.7387(8)	0.0130(6)
	Al	0.3375(2)	0.4139(3)	0.7405(9)	0.0125(7)

	O1	0.1960(7)	0.3931(7)	0.627(1)	0.020(2)
	O2	0.1267(6)	0.5590(6)	0.686(1)	0.027(2)
	O3	0.0578(7)	0.3721(6)	0.055(1)	0.014(2)
	O4	0.3193(6)	0.3613(6)	0.070(1)	0.017(2)
	Na1	2/3	1/3	0.084(1)	0.047(2)
	Na2	0.8761(3)	0.7530(3)	0.7774(7)	0.031(1)
	C1	0	0	0.92(1)	0.016(8)
	OC1	0.060(2)	0.119(1)	0.853(5)	0.045(4)
	C2	0	0	0.676(7)	0.016(8)
	OC2	0.062(2)	0.1228(5)	0.666(4)	0.045(4)
	Ow	0.311(3)	0.614(2)	0.146(3)	0.048(9)
6.63(3)	Si	0.0841(2)	0.4123(3)	0.7392(8)	0.0126(6)
	Al	0.3373(2)	0.4142(3)	0.7424(9)	0.0137(7)
	O1	0.1959(6)	0.3910(7)	0.626(1)	0.022(2)
	O2	0.1302(6)	0.5576(6)	0.687(1)	0.027(2)
	O3	0.0572(7)	0.3721(6)	0.061(1)	0.018(2)
	O4	0.3199(6)	0.3620(6)	0.073(1)	0.019(2)
	Na1	2/3	1/3	0.077(2)	0.065(3)
	Na2	0.8762(3)	0.7527(3)	0.7758(7)	0.034(1)
	C1	0	0	0.90(1)	0.031(8)
	OC1	0.061(4)	0.121(1)	0.854(5)	0.055(4)
	C2	0	0	0.684(8)	0.031(8)
	OC2	0.062(3)	0.1225(6)	0.661(4)	0.055(4)
	Ow	0.308(3)	0.615(2)	0.141(3)	0.045(9)

558

559

560 Table 4. Relevant bond distances (Å), ring "diameters" (Å), angles (°), areas (Å^2), volumes (Å^3) and
561 the (0001)-plane corrugation (Δz, Å) at different pressures.

562

P (GPa)	0.0001 P_0-DAC	0.76(2)	0.99(2)	1.39(2)	2.33(2)	3.59(2)	4.30(3)	5.00(2)	5.73(3)	6.16(2)	6.63(3)
Si-O1	1.613(9)	1.620(8)	1.603(8)	1.618(7)	1.610(7)	1.611(8)	1.607(7)	1.598(7)	1.604(9)	1.596(8)	1.610(7)
Si-O2	1.627(8)	1.631(8)	1.600(7)	1.617(7)	1.599(6)	1.607(8)	1.619(7)	1.601(7)	1.598(8)	1.629(7)	1.595(7)
Si-O3	1.612(8)	1.604(8)	1.611(7)	1.610(6)	1.617(7)	1.621(8)	1.609(7)	1.603(7)	1.624(8)	1.597(8)	1.616(8)
Si-O4	1.628(8)	1.624(9)	1.615(8)	1.622(7)	1.602(7)	1.615(8)	1.615(7)	1.613(7)	1.604(9)	1.612(8)	1.603(8)
<Si-O>	1.620	1.620	1.607	1.617	1.607	1.613	1.613	1.604	1.608	1.609	1.606
Al-O1	1.725(8)	1.723(8)	1.728(8)	1.721(7)	1.711(7)	1.709(8)	1.706(7)	1.716(7)	1.723(8)	1.716(8)	1.703(7)
Al-O2	1.701(9)	1.701(8)	1.723(7)	1.713(7)	1.708(6)	1.719(7)	1.711(7)	1.711(7)	1.719(8)	1.687(8)	1.730(7)
Al-O3	1.752(9)	1.755(9)	1.741(8)	1.736(8)	1.727(7)	1.729(8)	1.727(8)	1.734(8)	1.729(9)	1.734(8)	1.718(8)
Al-O4	1.734(8)	1.718(8)	1.734(8)	1.731(7)	1.742(7)	1.704(8)	1.715(8)	1.716(8)	1.708(9)	1.702(8)	1.697(9)
<Al-O>	1.728	1.724	1.732	1.725	1.722	1.715	1.715	1.719	1.720	1.710	1.712
Na1-O1 (x 3)	2.888(8)	2.883(8)	2.879(8)	2.886(7)	2.867(7)	2.894(7)	2.902(7)	2.874(7)	2.931(8)	2.914(7)	2.932(7)
Na1-O2 (x 3)	2.441(7)	2.397(6)	2.403(6)	2.38(6)	2.374(6)	2.312(6)	2.286(7)	2.291(6)	2.262(7)	2.252(6)	2.219(6)
Na1-Ow'	2.28(2)	2.26(2)	2.34(2)	2.25(2)	2.23(2)	2.25(1)	2.24(1)	2.25(1)	2.19(2)	2.20(2)	2.18(1)
Na1-Ow"	2.92(2)	2.94(2)	2.90(2)	2.91(2)	2.90(2)	2.83(1)	2.81(1)	2.79(1)	2.82(2)	2.79(2)	2.79(1)
Na2-O1	2.515(9)	2.479(8)	2.467(8)	2.432(7)	2.425(6)	2.371(7)	2.353(7)	2.337(6)	2.294(8)	2.301(7)	2.280(7)
Na2-O3'	2.436(9)	2.426(9)	2.419(8)	2.406(7)	2.397(6)	2.357(7)	2.351(7)	2.334(7)	2.310(8)	2.329(7)	2.308(7)
Na2-O4'	2.429(9)	2.437(8)	2.390(8)	2.375(7)	2.359(6)	2.355(7)	2.327(7)	2.324(7)	2.315(8)	2.316(7)	2.308(7)
Na2-O3"	2.930(10)	2.980(9)	2.902(8)	2.947(8)	2.949(8)	2.995(8)	2.999(8)	2.985(8)	3.040(10)	3.043(9)	3.051(9)
Na2-O4"	2.903(9)	2.905(9)	2.884(8)	2.910(7)	2.902(7)	2.940(7)	2.940(7)	2.937(7)	2.976(8)	2.960(7)	2.964(8)
Na2-Oc1'	2.40(3)	2.42(3)	2.34(4)	2.38(3)	2.26(3)	2.44(3)	2.27(3)	2.25(3)	2.30(3)	2.30(3)	2.31(5)
Na2-Oc1"	2.44(3)	2.38(3)	2.41(3)	2.43(3)	2.46(3)	2.23(3)	2.14(3)	2.39(3)	2.32(3)	2.31(3)	2.29(5)
Na2-Oc1"'	2.42(3)	2.44(3)	2.56(3)	2.42(3)	2.48(2)	2.50(3)	2.43(3)	2.49(2)	2.45(3)	2.47(2)	2.44(3)
Na2-Oc2'	2.39(2)	2.37(2)	2.41(3)	2.38(2)	2.29(2)	2.41(3)	2.28(3)	2.31(2)	2.30(3)	2.33(2)	2.33(4)
Na2-Oc2"	2.43(2)	2.43(2)	2.46(3)	2.42(2)	2.45(2)	2.34(3)	2.42(3)	2.40(2)	2.36(3)	2.34(2)	2.34(4)
Na2-Oc2"'	2.45(2)	2.44(2)	2.37(2)	2.42(2)	2.40(2)	2.34(2)	2.37(2)	2.32(2)	2.32(2)	2.31(2)	2.29(2)
C1↔C1, C2↔C2	2.542(2)	2.529(2)	2.538(3)	2.517(1)	2.503(1)	2.477(1)	2.468(2)	2.453(1)	2.438(1)	2.432(1)	2.422(1)
C1↔C2	3.85(7)	3.8(1)	3.81(9)	3.63(7)	3.71(7)	3.55(8)	3.56(6)	3.72(6)	3.59(8)	3.60(6)	3.46(7)
6mR⊥[0001]											
ω1	136.0(5)	137.5(5)	137.4(4)	138.2(4)	137.9(4)	141.4(5)	142.7(4)	141.5(4)	144.9(5)	144.9(5)	146.9(4)
ω2	100.8(4)	99.1(3)	99.5(4)	98.3(3)	98.7(3)	95.1(3)	94.0(3)	95.0(3)	92.0(4)	92.1(3)	89.9(3)
α	8.8(2)	9.6(2)	9.5(2)	10.0(2)	9.8(2)	11.6(2)	12.2(2)	11.6(2)	13.2(2)	13.2(2)	14.3(2)
O1↔O2	5.29(1)	5.24(1)	5.24(1)	5.23(1)	5.20(1)	5.15(1)	5.14(1)	5.119(9)	5.14(1)	5.11(1)	5.08(1)
Area	18.2(4)	17.8(4)	17.8(4)	17.7(4)	17.5(4)	17.1(4)	17.0(4)	16.8(4)	16.9(4)	16.7(4)	16.5(4)
4mR											

O3↔O4	4.15(1)	4.08(1)	4.13(1)	4.09(1)	4.07(1)	3.99(1)	3.97(1)	3.98(1)	3.91(1)	3.89(1)	3.87(1)
O2↔O2	3.56(1)	3.60(1)	3.584(9)	3.591(9)	3.563(8)	3.625(8)	3.63(8)	3.604(8)	3.625(9)	3.629(9)	3.677(9)
Area	7.39(6)	7.34(4)	7.40(4)	7.34(4)	7.25(3)	7.23(3)	7.21(3)	7.17(3)	7.09(4)	7.06(4)	7.11(4)
12mR											
O1↔O1	9.16(1)	9.12(1)	9.08(1)	9.04(1)	9.00(1)	8.88(1)	8.81(1)	8.837(9)	8.68(1)	8.70(1)	8.636(9)
O3↔O4	8.48(1)	8.51(2)	8.41(1)	8.432(9)	8.388(8)	8.405(8)	8.380(8)	8.351(8)	8.377(9)	8.386(8)	8.379(8)
(O1↔O1)/(O3↔O4)	1.038(3)	1.030(4)	1.037(3)	1.030(2)	1.031(2)	1.015(2)	1.009(2)	1.017(2)	0.994(2)	0.996(2)	0.989(2)
6mR//[0001]											
O3↔O3	4.97(1)	4.98(1)	4.94(1)	4.95(1)	4.93(1)	4.92(1)	4.91(1)	4.88(1)	4.89(1)	4.90(1)	4.89(1)
O4↔O4	4.95(1)	4.95(1)	4.92(1)	4.91(1)	4.88(1)	4.89(1)	4.87(1)	4.86(1)	4.86(1)	4.85(1)	4.85(1)
ε cage											
κ (O2-O2-O2)	91.1(3)	89.3(2)	90.2(2)	89.0(2)	89.3(2)	86.2(2)	85.7(2)	85.8(2)	84.5(2)	84.2(2)	82.4(2)
O2↔O2	8.47(1)	8.51(1)	8.45(1)	8.47(1)	8.42(1)	8.48(1)	8.48(1)	8.44(1)	8.46(1)	8.46(1)	8.51(1)
Δz	0.90(2)	0.86(2)	0.88(1)	0.84(1)	0.80(1)	0.74(1)	0.72(1)	0.70(1)	0.62(1)	0.64(1)	0.61(1)
V_{ch}	298(1)	296(1)	292(1)	289.4(8)	285.0(7)	278.7(7)	274.6(8)	273.0(7)	267.1(7)	267.5(7)	264.1(7)
V_{cg}	157(3)	155(2)	154(3)	153(2)	151(2)	150(2)	150(2)	147(2)	149(2)	147(2)	148(2)

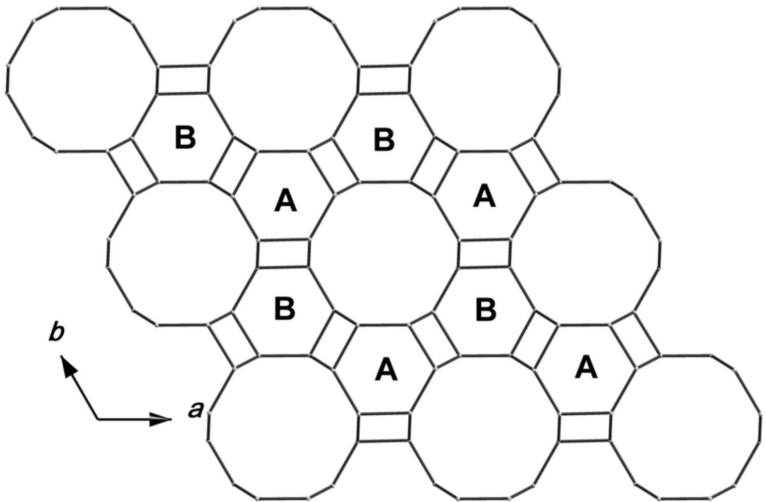
B
B
A
A
B
B
A
A
b
a

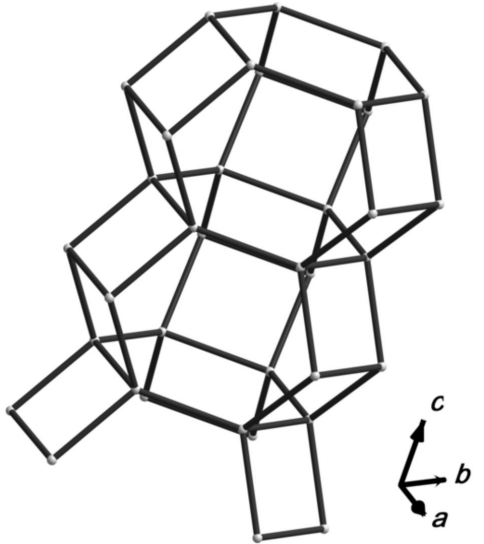
c
b
a

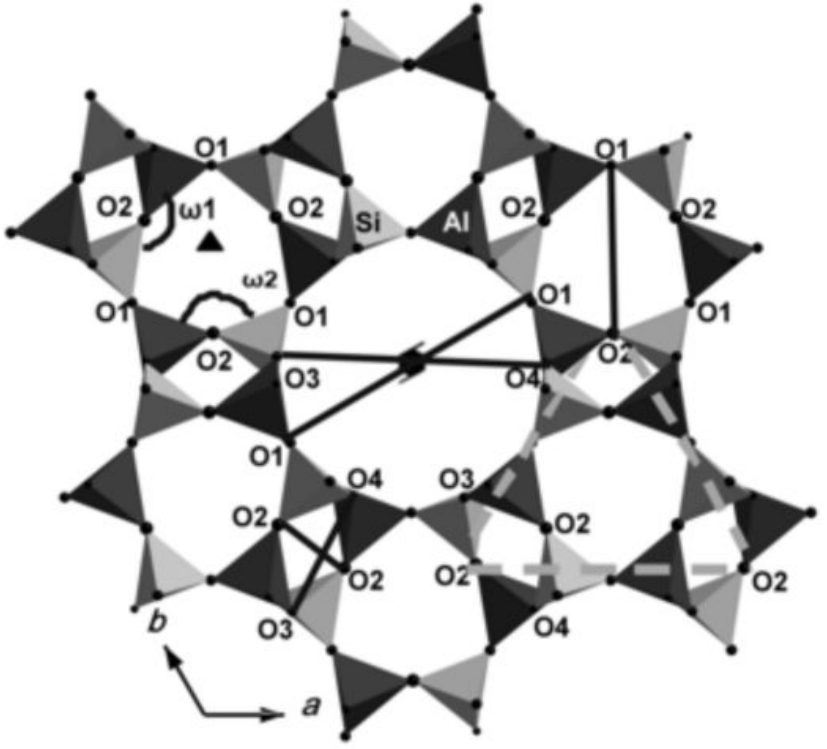
O1
O2
ω1
Si
Al
ω2
O3
O4
b
a

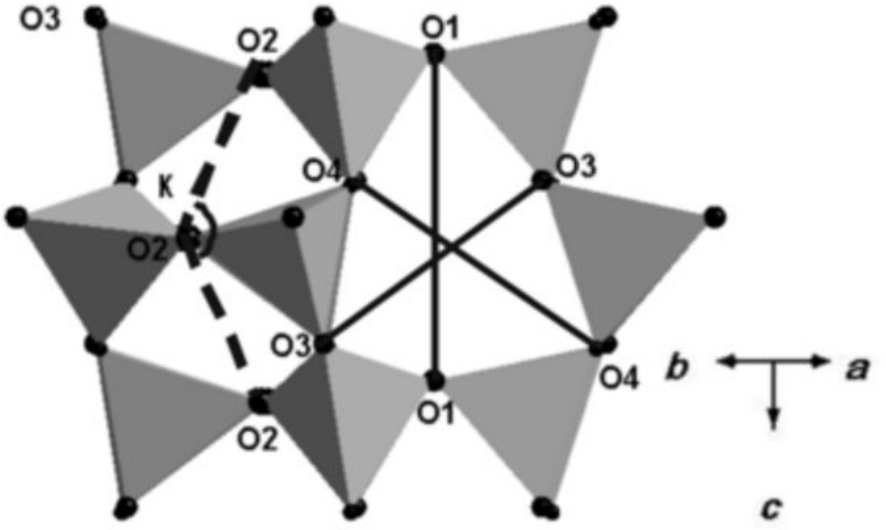
O3
O2
O1
K
O4
b
a
c

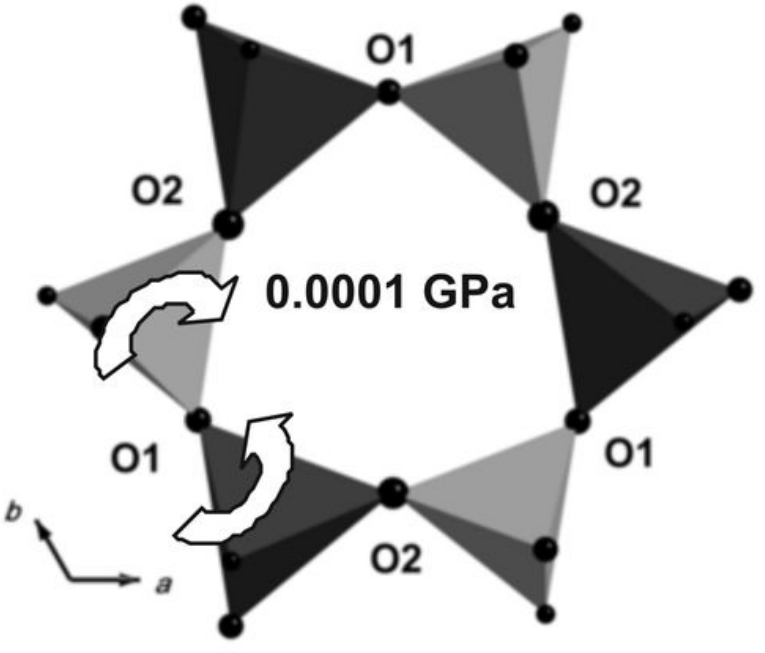
O1
O2
0.0001 GPa
b
a

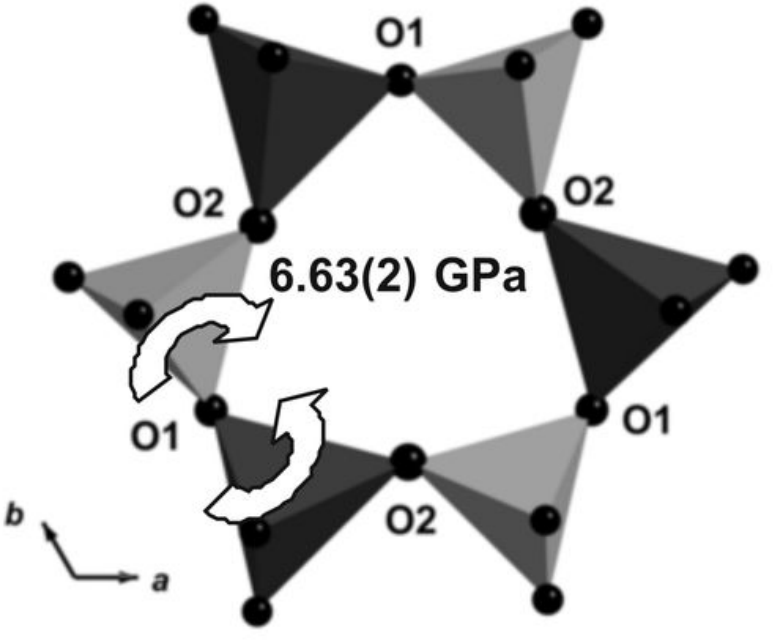
O1
O2
6.63(2) GPa
b
a

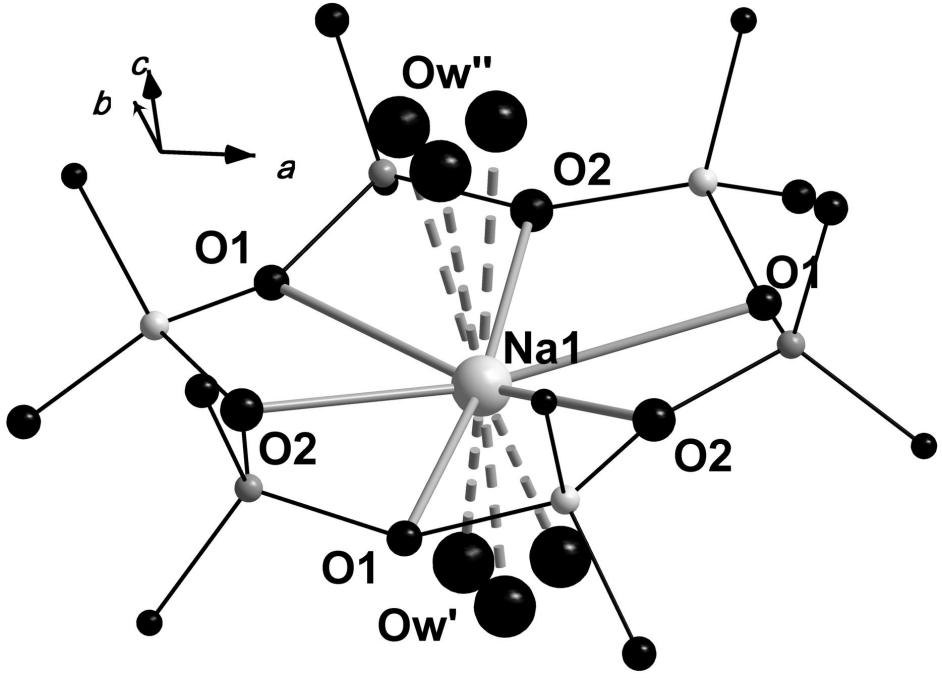
c
b
a
Ow''
O2
O1
O1
Na1
O2
O2
O1
Ow'

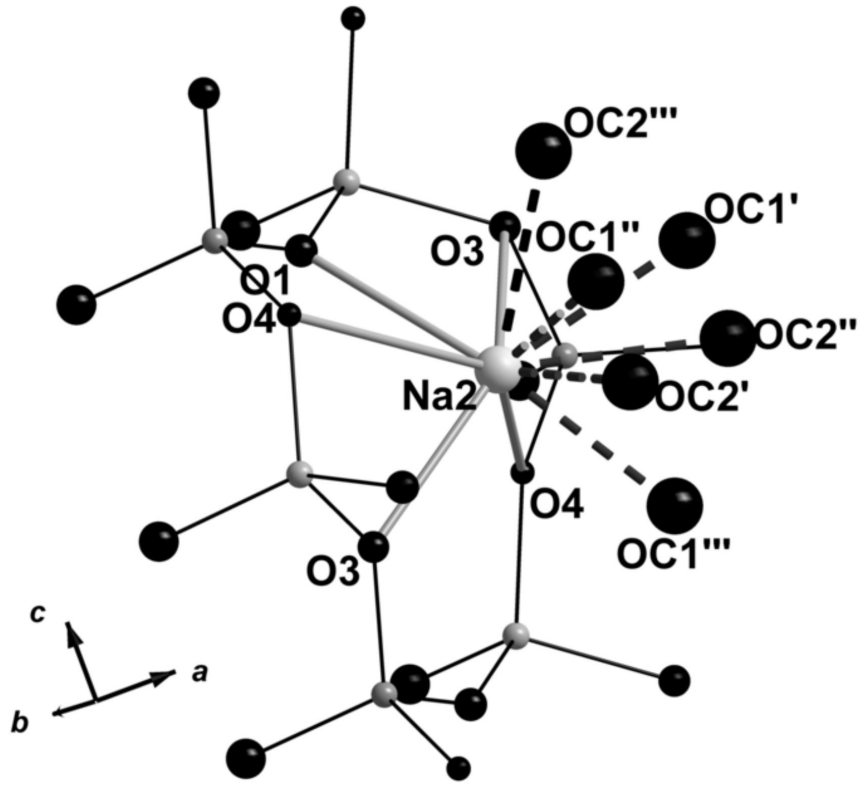
OC2'''
OC1'
O3
OC1''
O1
O4
OC2''
Na2
OC2'
O4
OC1'''
O3
c
a
b

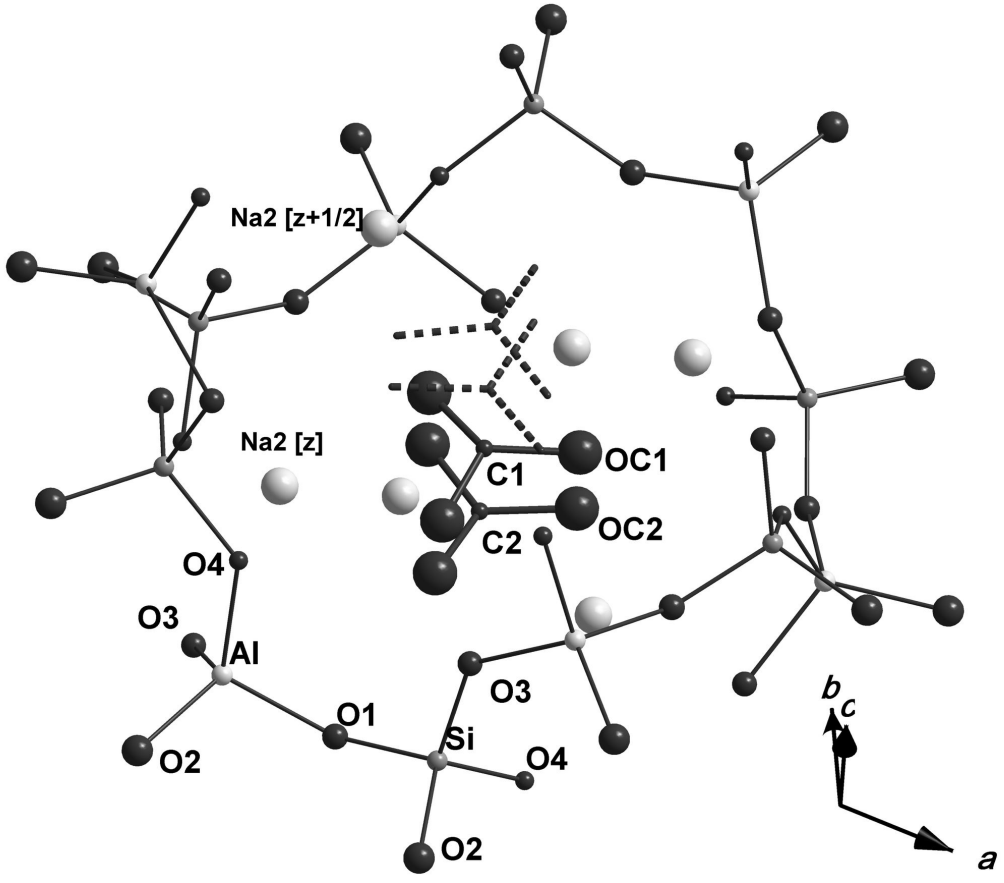
Na2 [z+1/2]
Na2 [z]
C1
OC1
C2
OC2
O4
O3
Al
O1
O2
Si
O3
O4
O2
b
c
a

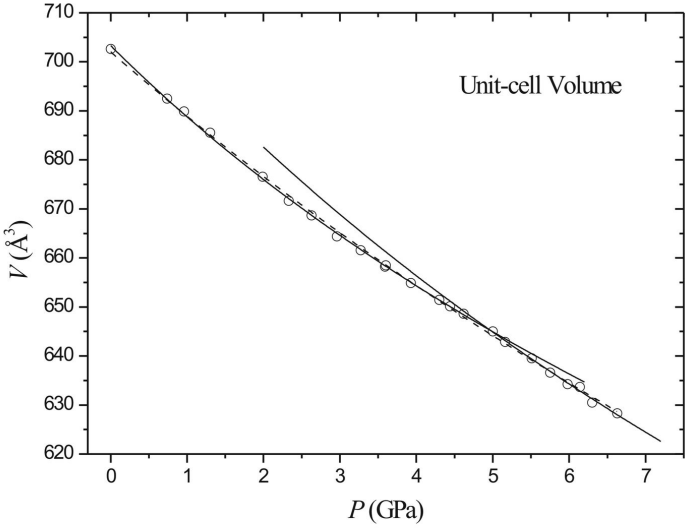
Unit-cell Volume
V (Å3)
P (GPa)

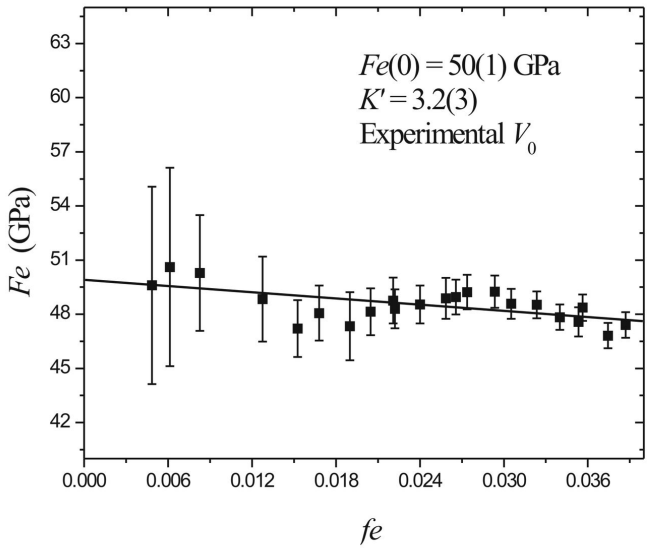
Fe(0) = 50(1) GPa
K' = 3.2(3)
Experimental V0
Fe (GPa)
fe

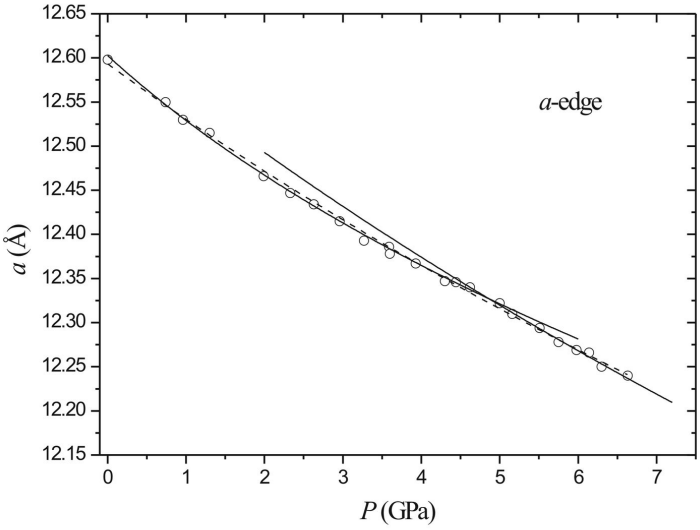
a-edge
a (Å)
P (GPa)

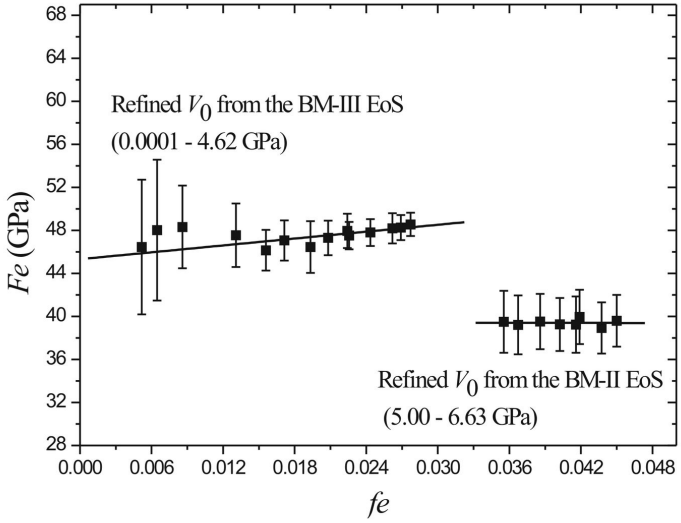
Refined V0 from the BM-III EoS
(0.0001 - 4.62 GPa)
Refined V0 from the BM-II EoS
(5.00 - 6.63 GPa)
Fe (GPa)
fe

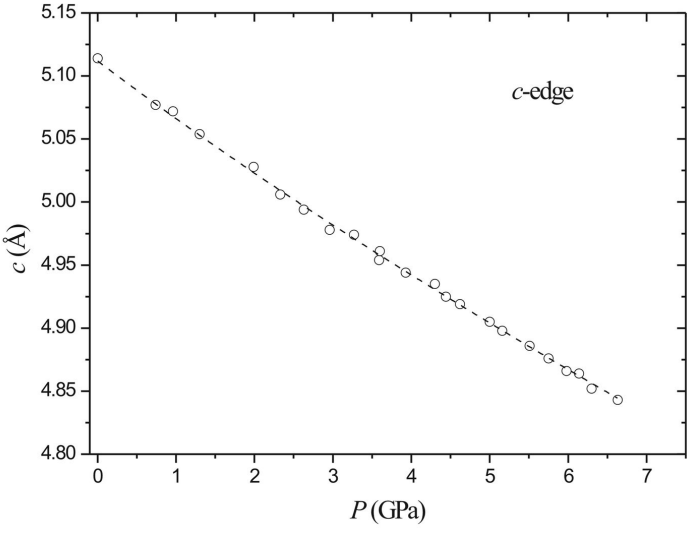
c-edge
c (Å)
P (GPa)

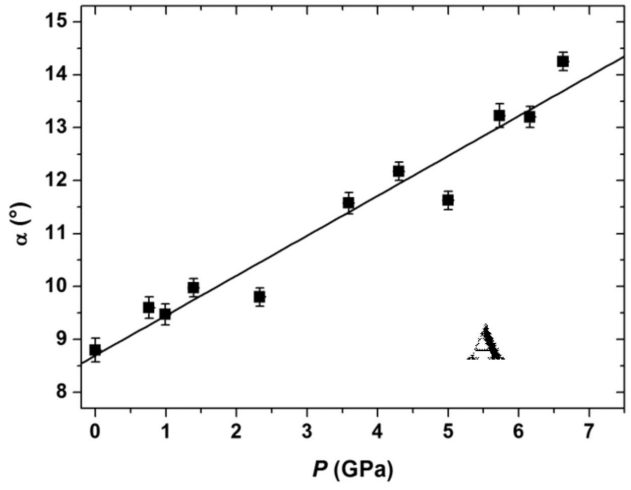
α (°)
P (GPa)
A

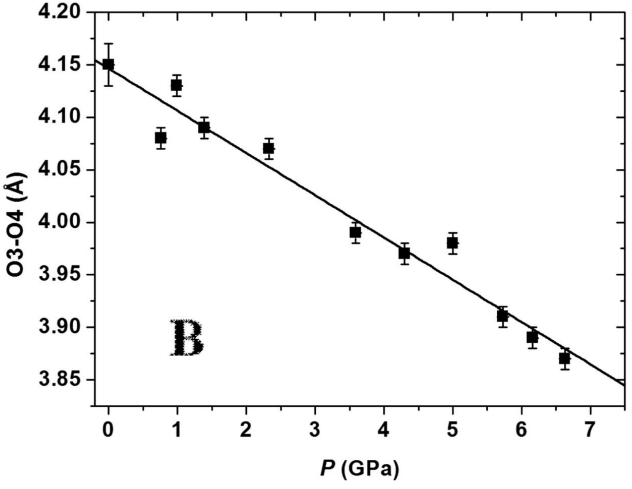
O3-O4 (Å)
P (GPa)
B

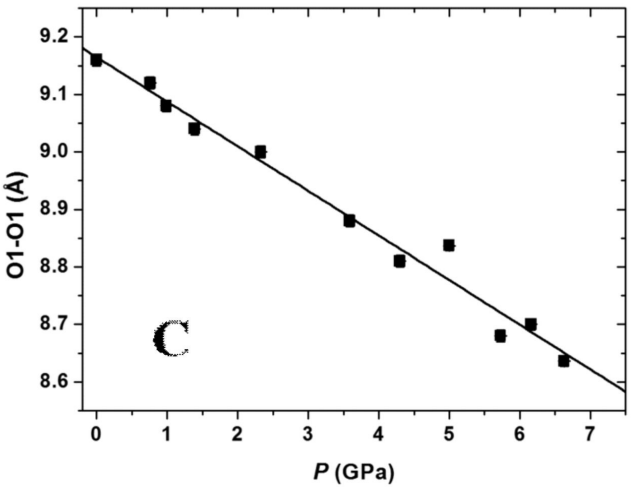
O1-O1 (Å)
P (GPa)
C

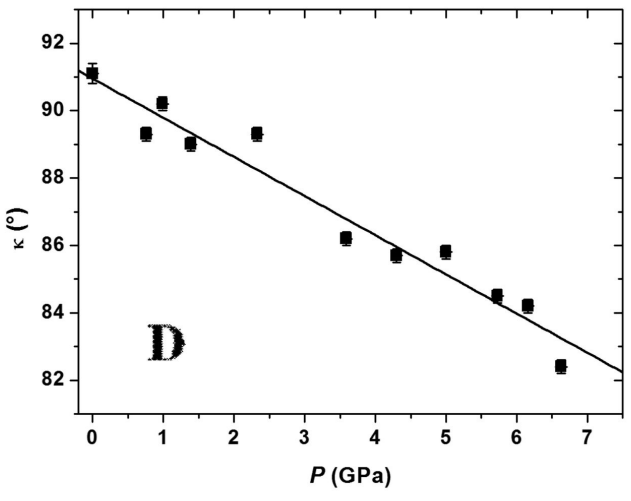
κ (°)
P (GPa)
D